SYRUP:

A NOVEL INVERSION METHOD FOR AEROSOL SIZE-DISTRIBUTION PROPERTIES FROM OPTICAL AND CHEMICAL MEASUREMENTS OF $PM_{2.5}$

by:

Paul Bissonnette

Submitted in Partial Fulfillment of the Requirements

for the Degree of Master of Science

at

Dalhousie University

Halifax, Nova Scotia July, 2019

DEDICATIONS

In Gratitude to all of my Past Mentors. Most Importantly, My Mother.

In Loving Thanks to My Partner, Kaitlyn. For the Endless Love and Support on an Uncertain Journey.

In Memory of Mitchel & Richard.

Rest in Peace, my Friends.

TABLE OF CONTENTS

LIST OF TABLES

LIST OF FIGURES

ABSTRACT

Accurate knowledge of aerosol mass scattering efficiency (α_{sp}) is essential to the realistic simulation of aerosol radiative forcing effects on climate as well as to the visibility influences of aerosols and also to the interpretation of satellite data. The comparison between measurement and simulation of α_{sp} may act as a prognostic factor in determining how accurately a model is representing optical characteristics and size-distribution parameters for aerosols. This study deals with improving representation of the latter parameters through the development of an inversion algorithm of α_{sp} which yields size-distributions. Through the deployment of 5 measurement sites across Canada the measurement of $PM_{2.5}$ (Particulate matter under a mean diameter of 2.5 μm) mass and chemical composition through filter-sampling stations was conducted from 2017 to 2019. Concurrently at all sites a 3-wavelength integrating nephelometer measured ambient scattering. By performing a multiple linear regression (MLR) on the data-set, the α_{sp} values for the 5 bulk chemical components of $PM_{2.5}$ are derived. Utilizing the wavelength sensitivity of α_{sp}, an algorithm is developed that inverts the measurements for aerosol size-distribution properties. The dry geometric mean diameter (D_{pg}) of organics, secondary-inorganics, black carbon, sea-salt, and dust is found to be 0.56, 0.62, 0.54, 0.46, and 0.51 μm, respectively. The variance of these distributions (σ_g), ordered as above, is found to be 1.45, 1.30, 1.28, 1.61, and 1.63, respectively (Unitless). The increases in dry diameter compared to values previously used in radiative transfer models is corroborated by the results of scanning mobility particle sizer data. These revised representations of aerosols size-distributions will enable more accurate modeling of radiative processes involving aerosols.

LIST OF ABBREVIATIONS AND SYMBOLS USED

BC ..... **B**lack **C**arbon

CABM ..... **C**anadian **A**erosol **B**aseline **M**easurement program

CTM ..... **C**hemical **T**ransport **M**odel

ECCC ..... **E**nvironment and **C**limate **C**hange **C**anada

GADS ..... **G**lobal **A**tmospheric **D**ata-**s**et

GEOS-Chem ..... Geochemical transport model

GFED ..... **G**lobal **F**ire **E**missions **D**atabase

GRASP ..... **G**eneralized **R**etrieval of **A**erosol and **S**urface **P**roperties

HPLC ..... **H**igh **P**recision **L**iquid **C**hromatography

ICP-MS ..... **I**nductively **C**oupled **P**lasma **M**ass-**S**pectrometry

ICARTT ..... **I**nternational **C**onsortium for **A**tmospheric **R**esearch on **T**ransport and **T**ransformation

IMPROVE ..... **I**nteragency **M**onitoring of **Pro**tected **V**isual **E**nvironments

MAPLE ..... **M**ortality **A**ssessment in low **P**articu**l**ate **E**nvironments

MLR ..... **M**ultiple **L**inear **R**egression

NAPS ..... **N**ational **A**ir **P**ollution **S**urveillance network

POM ..... **P**articulate **O**rganic **M**atter

SIA ..... **S**econdary **I**norganic **A**erosols

SS ..... **S**ea-**s**alt

SYRUP ..... **S**ize-distribution **Y**ielding **R**egression for **U**rban **P**$M_{2.5}$

TOMAS ..... The **T**w**O**-**M**oment **A**erosol **S**ectional microphysics model

α_{sp} ..... Mass scattering efficiency

D_{pg} ..... Geometric mean diameter

σ_g ..... Distribution variance

b_{sp} ..... Light scattering due to particle interactions

$PM_{2.5}$ ..... Particulate Matter with a diameter of 2.5 μm or smaller

PM_{10} ..... Particulate Matter with a diameter of 10 μm or smaller

f(RH) ..... Humidity based growth rate of scatter

Q_{scat} ..... Particle scattering efficiency

R_{eff} ..... Effective radius of a distribution

T_s ..... Triplet Spacing

ψ ..... Nephelometer Truncation Factor

CHAPTER 1 INTRODUCTION

The ability of aerosols to interact with radiation and thus to affect climate-forcing as well as their ability to negatively impact human health has lead to a deep and diverse literature on a multitude of physicochemical properties of aerosols. There exists an interesting intersection between the climate and health impacts of aerosols namely in the accurate determination of ambient aerosol concentrations that are required to study the epidemiological implications of exposure often utilize satellite remote sensing to fill in the informational gaps that are left from the sparse density of ground-based aerosol monitoring [1]. In order to accurately determine the aerosol concentrations from satellite optical measurements, in-depth knowledge of how aerosols interact with radiation is required [1–4]. Current epidemiological research points toward $PM_{2.5}$ (particulate matter under a mean aerodynamic diameter of 2.5 μm) as the most damaging size-fraction of particulate matter to human health [5–8].

This study focuses its investigation of the optical, chemical, and physical properties of aerosols to those under 2.5 μm in diameter, or $PM_{2.5}$ as it shall henceforth be referred. One of the most important factors to understanding aerosol-radiation interactions is the mass scattering efficiency (α_{sp}). α_{sp} can be defined as the amount of scattering that occurs at a given wavelength of incident radiation, $b_{sp,\lambda}$ (Mm^{-1}), divided by the aerosol concentration ($\mu g/m^3$), which yields α_{sp} in units of m^2/g. There are a number of factors that influence the mass scattering efficiency of an aerosol distribution; the chemical composition will determine the refractive index, the hygroscopic properties of the aerosol as well as the density of the aerosol. The factor that will be the focus of this study is the relationship that exists between α_{sp} and the size-distribution of aerosol particles. For particles in the Mie scattering regime (diameter $\approx 1\mu$m at visible wavelengths of light) there exists a strong relationship between particle size

and the amount of scattering that occurs at a given incident wavelength [9, 10]. Thus how the aerosol particles are distributed amongst different sizes will influence the amount of light scattering that occurs for a constant mass of aerosol. Lognormal distributions are a mathematically parsimonious description of aerosol size-distributions that have been shown to agree well with measured distributions; they will be adopted as the framework for representing distributions in this study [11]. The geometric mean particle diameter, D_{pg} (μm), describes the central tendency of the distribution of particles and the dispersion of the distribution is given by the variance, σ_g (Unitless). A distribution with a σ_g value of 1 would be mono-disperse in nature, with all particles having the same diameter, as σ_g increases, the spread in particle sizes about the mean value also increases. In more precise terms, the lognormal distribution can be described as in equation **??**. D_p^i is the diameter of a given size-grouping of particles, N(D_p^i) is the number density of particles of size D_p^i, and as before D_{pg} and σ_g represent the geometric mean diameter and the variance, respectively.

Insights given in the work of Hansen and Travis in the 1970's describe the importance of minimizing the number of variables required to describe a size-distribution to facilitate in the inversion of radiation measurements [12]. In the context of interaction with radiation, the single most relevant parameter to describe a size-distribution is the mean radius weighted by scattering, which is equivalent to the area weighted mean radius, or the effective radius as it is termed (R_{eff}). The effective radius is calculated as in equation 2, where r is the particle radius and n(r) is the number of particles at that radius.

$$R_{eff} = \frac{\int_0^\infty \pi \cdot r^3 \cdot n(r) dr}{\int_0^\infty \pi \cdot r^2 \cdot n(r) dr} \tag{2}$$

There exist a multitude of experimental methods to determine mass-scattering efficiency in the literature. In 2007 J. Hand et al conducted an extensive and in-depth review of the measurement of α_{sp} from over 60 short-term studies from 1990-2007 where they synthesize four categorical groupings of these methodologies which will be adopted here [13]. The first method is termed the theoretical approach, though the authors of this work find that name to be lacking in descriptive clarity as it still requires the measurement of particle size-distributions, as such it is not a purely theoretical approach. Therefore, this method shall be referred to as the size-resolved method in this work. In this approach the measurement

of particle mass or size distributions with any sufficiently sensitive instrument such as an optical particle counter (OPC) or scanning-mobility particle sizer (SMPS) provides sufficient information paired with several key assumptions to use Mie scattering theory to determine the α_{sp} value of a particle distribution. The key assumptions of this approach are that the chemical composition must be inferred from prior knowledge as well as assumptions of the particles optical properties and the mixing state of the aerosols must be made. The size-resolved method relies on the scattering budget described in equation 3, where D_p is the particle's diameter, $Q_{scat}(n_i, D_p, \lambda)$ is the scattering efficiency for a particle of a given species, n_i, at a specific diameter D_p and for a specific wavelength of incident light λ, and finally $F_{n,i}$ describes the distribution of particle number density of a chemical species at a given size. Integrating this expression over all relevant sizes will yield the α_{sp} for that aerosol plume. This method is considered to be the most accurate at discerning α_{sp}, as it has been shown to be incredibly accurate at recreating fine-time resolved scattering measurements[14]. However, the analytical precision and instrumentation required for this technique impede its implementation in long-term measurement programs, so it is also amongst the least utilized technique in the α_{sp} literature [13–15]. A more direct and operationally parsimonious technique to determine α_{sp} is often termed the direct measurement approach. While α_{sp} is not a directly observable property, it can be probed through separate measurements of aerosol mass through filter-based sampling and light scattering through an instrument such as a nephelometer. Equation 4 describes the system of equations that is solved for in this method to give $\alpha_{sp,\lambda}$, where $b_{sp,\lambda}$ is scattering at a given wavelength, and M is the total mass concentration of $PM_{2.5}$ determined by either gravimetric or mass-closure through summing the masses of the chemical components. It should be noted that this technique does not possess the ability to discern the α_{sp} values for individual chemical components of $PM_{2.5}$, rather it solves for a single α_{sp} for a given aerosol mixture. There have been attempts by researchers to extend the capabilities of this approach to solve for the α_{sp} values of individual species [16]. This was accomplished by Latimer et al using chemical speciation data and an arbitrary threshold of 60 % of the fractional mass of $PM_{2.5}$ to then attribute the α_{sp} of such measurements to be due entirely to the

$$b_{sp,i} = \int_0^\infty \frac{\pi}{4} \cdot D_p^2 \cdot Q_{scat}(n_i, D_p, \lambda) \cdot F_{n,i}(D_p) dD_p \tag{3}$$

species in question [16]. Such an approach would begin to converge to the true α_{sp} of a chemical species as the fractional mass approaches 1 for a given measurement, however true field measurements are hardly ever so compositionally simple. Different methods are required to more accurately parameterize the α_{sp} values of different chemical species in $PM_{2.5}$ such that compositional information from filter data is maximized rather than minimized.

$$\alpha_{sp,\lambda} = \frac{b_{sp,\lambda}}{M} \tag{4}$$

The final method of determining α_{sp} that will be discussed here is an extension of the direct measurement approach, but incorporates a multiple linear regression (MLR) to solve for the α_{sp} values of different chemical species. The assumptions underlying this approach are that all relevant species are accounted for in the scattering budget in equation 5, the mixing state of the aerosol must be assumed, and finally the different chemical species must be uncorrelated with each other [13, 17].

$$\begin{aligned} b_{sp} = f(RH)_{SIA} \cdot \alpha_{SIA} \cdot [SIA] + f(RH)_{POM} \cdot \alpha_{POM} \cdot [POM] \\ + \alpha_{Dust} \cdot [Dust] + \alpha_{BC} \cdot [BC] + f(RH)_{SS} \cdot \alpha_{SS} \cdot [SS] \end{aligned} \tag{5}$$

Mass closure studies that compare the gravimetric mass to the mass obtained from summing the masses of the 5 species listed above indicate that this assumption is a fairly accurate one at representing the bulk composition of $PM_{2.5}$ [18, 19]. If the measured scattering is fully explained by equation 5, then a system of equations may be set-up where b_{sp} is the independent variable in the system and the aerosol mass concentrations of each species represent the dependant variables. The resultant correlation coefficients that are found are interpreted to be the α_{sp} values for each species. Vasconcelos et al performed a critical review of the MLR technique for apportioning extinction (scattering + absorption) by aerosols wherein they identify the importance of constraining the effects of water-uptake [17] . Water does not appear as a term in equation 5 because the composition of $PM_{2.5}$ is often determined under temperature and humidity controlled conditions, so the amount of water present in this circumstance does not well correlate to the amount of water that would have been present in the aerosols when the scattering measurements were made at ambient temperature and relative humidity. As water is taken up by hygroscopic particles it results in an increase in cross-sectional area of a given particle, thus increasing the amount of scattering compared to the smaller dry particles. It is therefore necessary to account for the effects of water in the

system.

A commonly used method for describing aerosol hygroscopicity is the single-parameter kappa-kohler theory first proposed by Petters and Kreidenweiss that has since been adopted by others [18, 20]. In this method a single parameter κ is assigned to each species on the basis of its water uptake. Values for κ range from zero for hydrophobic species like dust, to over one for species like sea-salt. The volume-based growth factor is defined in equation 6, where V_{amb} refers to the volume under ambient RH, and V_{dry} is the particles volume at an RH of zero. α_w is the activity of water which may be approximated as $\alpha_{sp} =$ RH/100.

$$\alpha_w = 1 + \kappa * \frac{V_{amb}}{V_{dry}} \tag{6}$$

The κ values are then applied to create RH dependant volume-growth factors as in equation 7.

$$f(RH) \coloneqq \frac{V_{amb}}{V_{dry}} = 1 + \kappa * \frac{RH}{100 - RH} \tag{7}$$

For multi-component aerosols, a single κ value may be obtained by taking the volume-weighted average for all components. Using this information on how the aerosols size varies with ambient RH, it is possible to apply a correction factor to the measured ambient scatter to estimate the dry scatter. This correction factor is the inverse of the volume growth factor f(RH), multiplied by the ambient scatter giving the dry scatter as in equation 8.

$$b_{sp,dry} = \frac{b_{sp,amb}}{f(RH)} \tag{8}$$

Water-uptake by aerosols is not the only factor that should be considered as affecting the measured scattering. Nephelometers can give precise measurements of scattering, however there are also well documented non-idealities that must be considered when using these instruments [21, 22]. The most well known of these non-idealities is the truncation error that exists due to the instruments insensitivity to measuring scattering over the full range of 0 to 180°, rather they tend to provide measurements only of only the region within 7-173 °. It is not possible to apply correction factors a priori to the scattering measurements due to the size-dependant nature of the scattering phase function, which describes the angular scattering patterns of particles, and therefore also determines the exact amount of that scattering that will not be measured in the angular exclusion zones of the instrument. Truncation correction factors

have in the past been directly applied to nephelometer measurements, using the angstrom exponent as a proxy for the measured particle sizes [21]. The angstrom exponent does not constitute a unique identifier for particle size, though it does serve as a useful proxy, the same angstrom exponent can be obtained for different particle sizes [23]. In this study the correction factors have been developed on the basis of mie theory as per Anderson et al's method, and are applied to directly to the theoretical calculations of scattering which are then used to interpret the non-truncation corrected scattering measurements from the nephelometer [22].

As the particle size-distribution is one of the dominant factors in controlling the observed α_{sp}, it is therefore an attractive goal to invert optical measurements to obtain the particle size-distributions so that more accurate modelling of the desired optical properties is possible. Seminal work has been done to address this problem by Benjamin Torres, Oleg Dubovik and colleagues in the development of the GRASP (Generalized Retrieval of Aerosol and Surface Properties) algorithm [2]. Notably, the GRASP algorithm has been regularly implemented by AERONET (Aerosol Robotics Network) to provide an array of aerosol micro-physical properties from ground based AOD (Aerosol Optical Depth) measurements. Additionally, the GRASP algorithm has been applied and validated by Espinosa et al in the determination of aerosol size-distributions from a polar nephelometer [24]. An essential component of the GRASP algorithm is the difference in extinction and scattering properties of aerosols at different wavelengths of analysis, which is made use of to over-come the double-valued inversion problem that is encountered for properties such as α_{sp} when attempting to invert for particle distribution size. However, the GRASP algorithm also requires information of the angular patterns of scattering and extinction in order to optimize inversion solution [2]. Information of the angular scattering patterns is retrieved from polar nephelometer measurements, but in the far more commonly used and less-expensive integrating nephelometer, knowledge of the angular scatting patterns is reduced to hemispheric patterns (forward-scatter and back-scatter), thus the GRASP algorithm cannot be used on data-sets from these instruments to retrieve particle size-distribution information. The sagacious insights of Dubovik to capitalize on the wavelength-dependence of scattering and absorption by aerosols to create an algorithm to invert for size-distributions can be used as the foundation upon which other size-inversion algorithms may be developed.

What is currently lacking in the literature is a reliable method to use integrating nephelometer data as well as filter-based measurements of $PM_{2.5}$ mass and composition to determine the size-distribution of the chemical species that constitute $PM_{2.5}$. This would enhance the accuracy of models to properly represent optical interactions with aerosols of different species. It is therefore the aim of this work to develop such an algorithm which can be though of in broad terms to be an extension of the multiple linear regression method of determining α_{sp}, paired with a theoretical mie-framework that is used to interpret the results based on the convergence of answers for the multiple wavelengths of measurement by the nephelometer. This approach differs to previous work such as from Latimer et al in that in that no boundary conditions are placed on particle sizes prior to analysis [16]. The result of this is a more fundamental approach to inverting for particle size-distribution parameters using measured α_{sp} values that must explicitly solve for the variance of the distribution as well as finding the true answer in a double valued inversion problem.

CHAPTER 2 METHODS

FILTER SAMPLING

To facilitate the investigation of the optical and chemical properties of $PM_{2.5}$ in Canada, 5 measurement sites were created at strategic locations across the country in Halifax NS, Sherbrooke QC, Downsview ON, Lethbridge AB, and Kelowna BC. These measurement sites were established at various times in 2017 and are set to complete sampling in the summer of 2019. At each of these sites a filter-sampling station to collect particulate matter onto Teflon filters was installed along with a three-wavelength integrating nephelometer unit that measures scattering due to aerosols. The sampling station are operated by site-operators at the local facilities where they were installed, on rooftops away from potential contamination sources. The filter sampling stations used in this study are the SS5 series instruments designed and manufactured by AirPhoton. The stations operate using pre-assembled plastic cartridges of 8 stretched Teflon filters that are inserted into the sampling station and then sample autonomously for a period of 54 days. Size-resolution is achieved in sampling through the use of a dynamic cyclone inlet that operates on the principal of variable flow-speed to induce the desired size-cut. A flow-speed of 5 lpm (liters per minute) is used to obtain a size-cut of $PM_{2.5}$, and a lower flow-rate of 1.5 lpm is used to induce the larger size-cut of PM_{10}. The sampling schedule is designed such that six filters sample $PM_{2.5}$, one filter samples PM_{10} and finally one filter acts as a traveling blank. The filters sampling $PM_{2.5}$ operate on duty cycles for 9-day sampling periods. That is to say, the filter does not sample continuously over the 9-day period, but rather samples a total of 48-hours and the time of day that sampling occurs rotates throughout the 9-day period, as is depicted in the figure 1. The single PM_{10} filter samples for the entire

54-day period to give an average PM_{10} concentration. The PM_{10} sampling occurs for exactly one hour following the completion of the $PM_{2.5}$ sampling. The time of day of sampling is designed so that the filter completes sampling at the end of a diurnal cycle so as to minimize the loss of semi-volatile species due to pulling warm air during the day-time over the filters. At the beginning and end of sampling the flow-rates of the sampling stations are measured both internally and externally using a flow-meter. The flow-rates are adjusted to meet the desired flow-rates of 5 lpm and 1.5 lpm for the two size-cuts of PM. The flow-rates are also measured at the end of the filter sampling to ensure that there has not been any major drift in the initial flow-rates that would cause the cartridge data to have to be discarded on the basis of inaccurate flow-rates leading to unreliable size-cuts in PM. A standard of $\pm$ 10% of the set-flow rate is used as the criteria for determining if a sampled cartridge meets flow-rate criteria for further analysis.

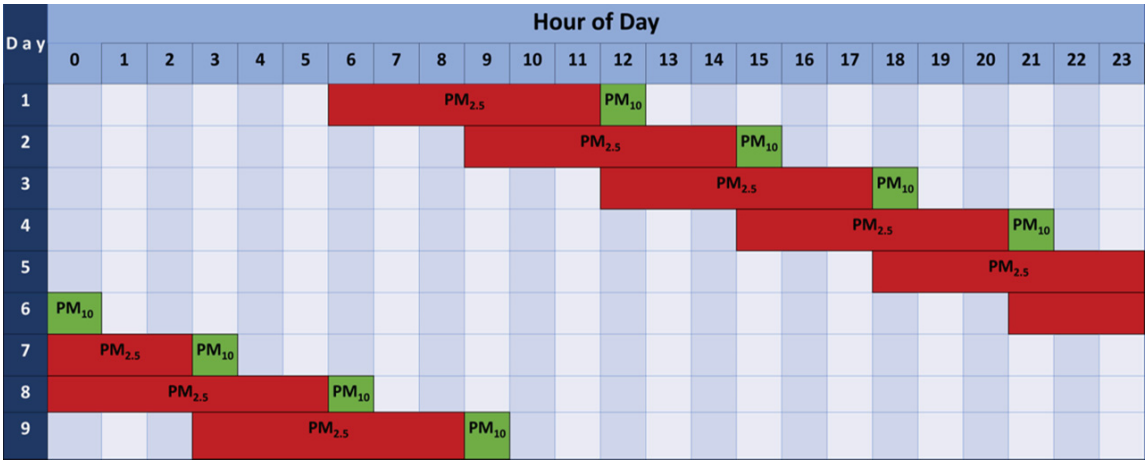

Figure 1: Filter Sampling Duty Cycle over 9-day Sampling Period

FILTER WEIGHING

Stretched PTFE® filters (MTL 2.5 μm pore-size) are pre and post-weighed in triplicate on a Sartorius Ultramicro balance with a weighing precision of $\pm$ 0.1 μg. Weighing is conducted in a cleanroom that is temperature controlled to 20-23 °C, and RH controlled to 30 $\pm$ 5 %. Filter masses are blank corrected to account for any mass deposited through means other than sampling.

BLACK CARBON

Using the procedure described by Snider et al, black carbon is measured using surface reflectance on the sampled filters with a Diffusion Systems EEL 43M smoke stain reflectometer [18].

ION-CHROMATOGRAPHY

Filters are extracted in 6 mL of deionized water (18-MOhm·cm) inside of a sonication unit for 1 hour at ambient temperatures. The filter is then removed from the extract and stored for later analysis. The extract is split into several aliquots, one of which is used for high-performance liquid chromatography (HPLC) analysis with an anion separation column on a Thermo Dionex ICS-1100 system to measure NO_3^{-1} and SO_4^{2-}. The second aliquot is used for HPLC analysis using a cation separatory column to measure NH_4^+, K^+, and Na^+. The last aliquot is saved for later analysis.

INDUCTIVELY-COUPLED PLASMA MASS SPECTROMETRY

Stretched Teflon filters are unable to be sectioned with any degree of precision due to the stretched membrane as was the method utilized by Snider et al [18]. Therefore, entire filters are extracted a second time for ICP-MS analysis to determine the concentration of the crustal-associated elements (Mg, Fe, Al and Zn) as well as other trace-metals (V, Ni, Cu, As, Se, Ag, Cd, Sb, Ba, Ce, Pb) in the collected $PM_{2.5}$. The first step of the analysis includes a high-temperature acid digestion in 6 mL of 20% trace-metal grade HNO_3 solution heated to a temperature of 97 °C for 2 hours in a temperature controlled heating block. The filter extracts are neutralized by dilution up to a volume of 10 mL using the third aliquot from the extraction for HPLC. This ensures that any highly soluble metals that may have been extracted during the sonication procedure are measured in this procedure. An analysis performed on the extraction efficiencies under several different acidity conditions would suggest that a negligible amount of metal is lost in the neutral-pH water sonication procedure. The sample extracts are submitted for quantitative analysis by inductively coupled plasma mass spectrometry (ICP-MS) on a Thermo Scientific X-Series 2 instrument. The analysis is performed using 5 concentrations of a 25-element acidic stock solution. Three reference

metal ions (In, Sc, and Tb) are used for atomic mass calibration. All of the ion mass signals are measured in triplicate and the mean signal is used for elemental quantification. Concentrations are blank corrected using lab-blanks that follow the same extraction protocols and lab-ware as stated above.

RECONSTRUCTION OF FINE MASS

When viewed from the context of the formation process that result in $PM_{2.5}$ it is relevant to consider the composition of $PM_{2.5}$ to be based on several compound classes or grouping. The chemical groupings used here are particulate organic matter (POM), secondary-inorganic aerosols (SIA), Black carbon (BC), sea-salt (SS), and finally also dust. Thus it is useful to reconstruct this fine-mass composition from the constituent measurable chemical components.

POM

Particulate organic matter was not measured explicitly in this analysis, rather this component is determined through a mass-closure approach with the gravimetrically determined mass and the other four components of $PM_{2.5}$ defined above.

SIA

SIA is considered in this study to consist of ammonium nitrate and ammonium sulfate. Ammonium sulfate is calculated assuming all of the measured sulfate-ion is associated with Ammonium sulfate in the form of $(NH_4)_2SO_4$. Ammonium nitrate is calculated assuming that all of the measured nitrate ion is neutralized by ammonium in the form NH_4NO_3. Ammonium nitrate and ammonium sulfate are then summed together to give the concentration of total SIA.

SEA-SALT

As described by Snider et al, sea-salt is calculated from the concentration of Na^+ corrected for crustal influences using the $[Mg^{2+}]$ concentration, multiplied by a factor of 2.54 to account for Cl^- in NaCl [18].

DUST

Dust, or crustal material as it is sometimes also referred, originates from a diverse number of sources ranging from road dust, soil, or suspended sand particles. As described by Snider et al, the approach of Malm et al is adapted such that dust is calculated as $10 \cdot [Al + Fe + Mg]$ [18, 25].

PARTICLE-BOUND WATER

Particle bound water is calculated using the kappa-values determined from the mass concentrations of the hygroscopic components and then determining the f(RH) at the measurement conditions to account for the amount of water that will remain bound to the $PM_{2.5}$ even at the low humidity conditions of the measurement clean-room. The stretched Teflon filters employed in this study are all batch tested, where 5 % of filters from a package are taken and analyzed through the HPLC and ICP-MS analysis protocols. If the background levels on a batch of filters is deemed to be too high or contaminated, the package of filters is not used in field sampling.

NEPHELOMETER MEASUREMENTS

A three-wavelength integrating nephelometer produced by AirPhoton was used to measure scatter at all of the sampling sites. The IN1002 series instrument that was used in this study is equipped with the same cyclone inlet used on the filter sampling stations. The size-cut of sampled $PM_{2.5}$ is therefore induced by changing the flow-rate from 5 lpm for $PM_{2.5}$ and 1.5 lpm for PM_{10}. The nephelometer operates on a much finer time-resolution, making measurements of total scatter as well as back scatter at 3 wavelengths (457, 532, 634 nm) every 15 seconds. The size-cut of sampling alternates between $PM_{2.5}$ and PM_{10} at a frequency of once every 30 minutes. The nephelometer also measures the ambient temperature and relative humidity inside of the sampling chamber during use.

NEPHELOMETER QA/QC

Due to the very different sampling protocols used by the nephelometers and the sampling stations, some criteria have to be applied to ensure that the values are comparable in terms of representing measurements of the same states of the atmosphere. The screening protocols implemented here are the same as those used by the IMPROVE network in screening their nephelometer data [16]. An upper-limit of scattering of 2500 Mm^{-1} is used, above which scattering values are screened out. Due to the significantly different temporal resolutions between the two instruments used, the filters are far less sensitive to sudden or transient changes to scatter. A derivative based screening protocol is used that screens out scattering values if there is a change in scattering that is greater than $\pm 50 Mm^{-1} hr^{-1}$. Owing to the highly non-linear growth of particles that occurs at RH values approaching 100 %, and the large divergence between different hygroscopic growth parameterizations at these RH values, nephelometer measurements are screened out if the ambient RH exceeded 90% [16].

SCATTERING CORRECTION FACTORS

The IN1002 system has yet to undergo a rigorous performance analysis as has been performed on more commonly utilized systems such as the Aurora3000 nephelometer. In an effort to accuracy of the measurements from the IN1002 nephelometer, a set of scattering correction factors were created from an inter-comparison that was performed between the previous generation of Airphoton nephelometer, the IN1001 series and the Aurora 3000 nephelometer. The correction factors are given as a function of angstrom exponent, which is a parameter that describes the spread between scattering measurements at different wavelengths of analysis. The angstrom exponent is correlated with the size of the particles being measured [23]. The total scattering shows very close agreement between instruments, with correction values close to 1. The back-scattering correction factors are more significant, being as large as 0.7 for small angstrom exponents. The scattering values were truncation corrected for both instruments, so these corrections should not be interpreted as differences in the nephelometer truncation factors between the two instruments, but are arising due to some unidentified non-idealities in the instrument.

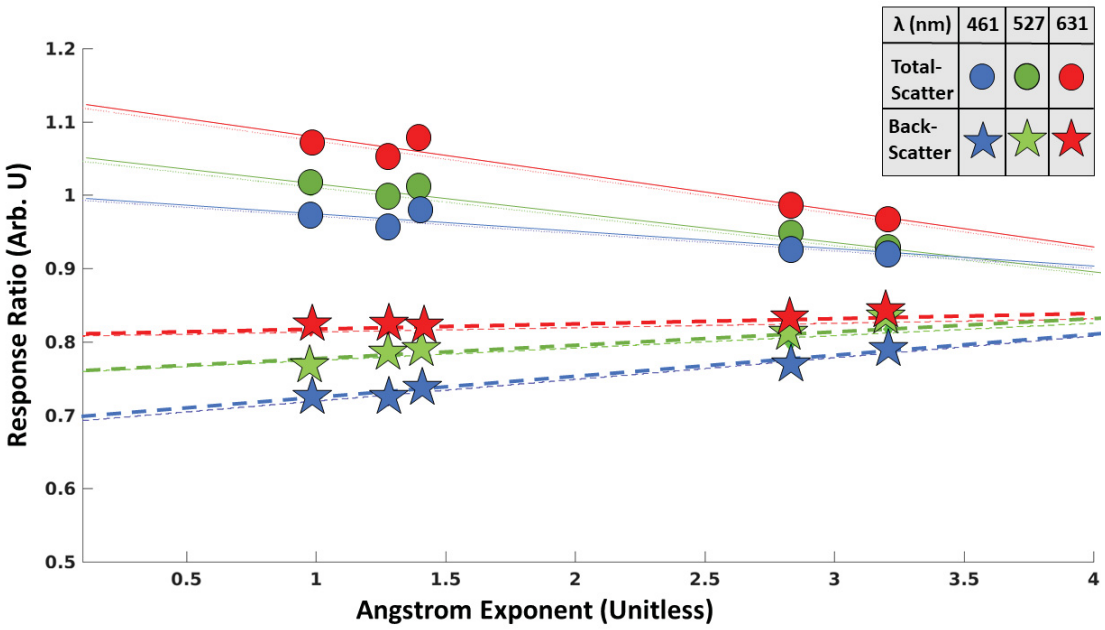

Figure 2: Figure of the wavelength dependant correction factors plotted vs angstrom exponent from IN1001 vs Aurora 3000 Nephelometer inter-comparison.

MASS SCATTERING EFFICIENCY

Mass scattering efficiency is calculated in line with the direct measurement method described by Hand et al, with the modification of adjusting the gravimetrically measured $PM_{2.5}$ mass to remove any residual water remaining in the aerosol at clean-room RH conditions [13]. α_{sp} is calculated using equation 9, where $PM_{2.5,dry}$ is the dry $PM_{2.5}$ mass concentration ($\mu g/m^3$) and $b_{sp,9day,\lambda_i}$ is the 9-day (1 filter) average scatter at each wavelength of measurement (450, 550, 650 nm).

$$\alpha_{sp,\lambda_i} = \frac{b_{sp,9day,\lambda_i}}{PM_{2.5,dry}} \tag{9}$$

The native measurement wavelengths of 436, 542, 634 nm are converted to scattering values at 450, 550, and 650 nm for ease of comparison of the α_{sp} with the more standardized wavelength of reporting in the literature of 550 nm. This transformation is accomplished through the calculated angstrom exponent for the set of scattering measurements, where the average of the 3 calculated angstrom exponents $(\lambda_1 - \lambda_2, \lambda_1 - \lambda_3, \lambda_2 - \lambda_3)$ is taken as the distribution angstrom exponent, this is then applied to the

scattering values as in equation 10.

$$b_{sp,\lambda} = b_{sp,\lambda_0} \cdot \left(\frac{\lambda}{\lambda_0}\right)^{-\alpha} \tag{10}$$

It was found that the α_{sp} values for a given filter were sensitive to the averaging window used to obtain a 9-day average b_{sp} value. Figure 3 depicts the variation that is observed across the α_{sp} values obtained for all filters when the full 9-day time-series of scatter is used (green line), compared to when the scattering is averaged over just the exact hours that the filter was sampling. It is presumed that the inhomogeneity in $PM_{2.5}$ concentration over the course of filter sampling, due to meteorological and less predictable adventitious factors results in the differences between the two average values of α_{sp}. The scattering over just the hours that the filter was sampling is taken to be more reflective of the $PM_{2.5}$ that was sampled onto the filter.

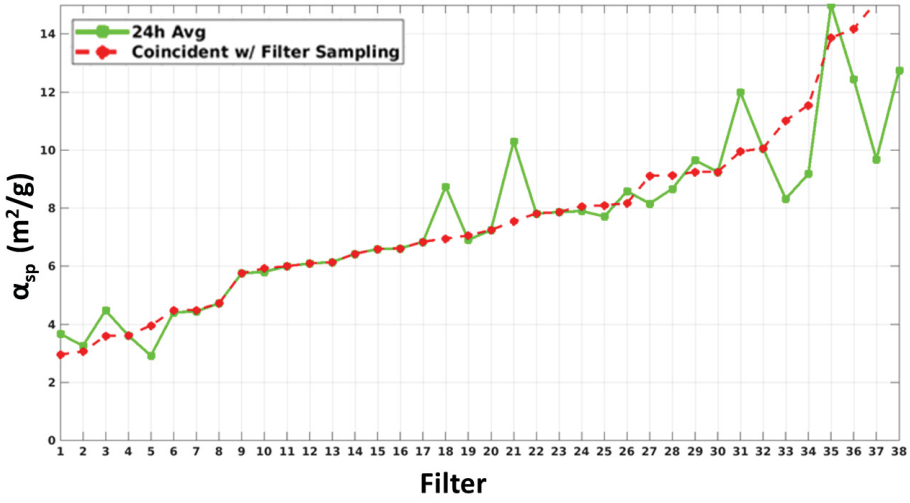

Figure 3: Example of the effects of diurnal patterns on intermittent sampling. Purely coincident (Red) is far more stable than the 24h avg values (Green)

MULTIPLE LINEAR REGRESSION

Three multiple linear regressions are performed on the measurement data-set using the α_{sp} values measured at three separate wavelengths. Using the MLR procedure outlined by both J. Hand and Vasconcales,

$$b_{sp} = \int_{1nm}^{10\mu m} \frac{\pi}{4} \cdot D_p^2 \cdot Q_{scat}(n, D_p, \lambda) \cdot F(D_{pg}, \sigma_g, D_p) dDp \tag{11}$$

the 9-day average scattering measurement is taken to be the independent variable in the regression system. The mass concentration of each of the five components of $PM_{2.5}$ for each filter are used as the dependant variables. A simple least squares regression is performed and the fit coefficients are interpreted as the α_{sp} values for each species. The measurements for all filters from all five of the measurement sites are compiled into a single data-set that the linear regression is performed on. After QA/QC on the data-set and being unable to use a number of filters due to a lack of concurrent scattering measurements due to malfunctioning nephelometers, this left 48 filters or 432 total days of measurements. The MLR technique as noted by J. Hand and Vasconcelos, is sensitive to the number of measurements that are used in the regression, so to maximize the size of the data-set and thus the stability of the α_{sp} values obtained from the MLR, all of the sites are compiled into a single data-set that the regression is performed on [13, 17].

SYRUP ALGORITHM

The development of an algorithm capable of inverting the optical and chemical measurements to obtain the particle size-distribution was accomplished through the development of the **S**ize-distribution **Y**ielding **R**egression for **U**rban **P**$M_{2.5}$ (SYRUP). In order to interpret the α_{sp} values for each species in terms of the more fundamental property of the size-distribution for each species, theoretical knowledge is required of how α_{sp} varies as a function of the two relevant parameters for the size-distribution of a lognormally distributed species. These are D_{pg} (μm), the geometric mean diameter of the distribution, as well as σ_g (Unitless), the variance of the distribution. Using Mie code developed by Bohren and Huffman, the scattering efficiency Q_{scat,λ_i} (Unitless), as well as the scattering phase function ($P(\theta)$) for spherical particles ranging in diameter from 1 nm up to 10um is calculated [26]. The refractive indexes of the five species and at each wavelength is taken from the global atmospheric data-set (GADS) for use in Mie calculations [27].

An array of size-distributions are then calculated for all five species of aerosols, varying D_{pg} from 0.01 um up to 3 um and varying the σ_g values from 1 (monodisperse aerosol) up to 2.5 (highly polydispersed aerosol). The scattering for the entire distribution is calculated as the sum of scattering over all D_p

values, expressed in equation 11 as the integral from 1 nm to 10um weighted by the number of particles of a given size in the distribution $F(D_p, D_{pg}, \sigma_g)$, with scattering efficiencies from Mie theory of Q_{scat} that are a function of the real part of the refractive index, n, calculated for a total number concentration of $N_t(\#/m^3)$.

The α_{sp} values are then calculated by taking the quotient of the scattering at each wavelength, for each distribution calculated above and dividing by the mass of particles in the distribution $M(D_{pg}, \sigma_g, \rho_{species})$. These are calculated using the same species densities as Latimer et al and the N_t value used in b_{sp} calculations [16]. For a σ_g value of 1.40 the theoretical curve of α_{sp} vs D_{pg} for POM is shown in figure 4. This illustrates one of the key problems of this inversion algorithm; how to discern which of the two solutions that could be obtained from intersections of the theoretical α_{sp} curves with the measured α_{sp} values for D_{pg} is the correct one. In the work of Latimer et al this double valued inversion problem was simplified by only considering solution set-1 [16]. Furthermore, assumption of the σ_g value to constrain the solution to a single lognormal size-distribution must be made. As can be seen in figure 5, distributions with different variance values (σ_g) have notable different theoretical α_{sp} curves. If the system of measurements is expanded to also include the solutions obtained from the two other wavelengths of measurement, 6 possible values for the D_{pg} are obtained which can be grouped into either solution 1 (left) and solution 2 (right). Depicted in figure 6 panel (a) and (c) are the inversion results at a distribution variance of 1.40; neither solution sets has the 3 wavelengths converging to give a single D_{pg} answer. Figure 6 panel (b) depicts the σ_g value for BC which results in convergence for solution set-2. In more rigorous terms, the triplet spacing is defined as the differences between D_{pg} inversion results summed in quadrature divided by the number of wavelengths of analysis (see equation 12).

$$T_s = \frac{\sqrt{(D_{pg,\lambda_1} - D_{pg,\lambda_2})^2 + (D_{pg,\lambda_1} - D_{pg,\lambda_3})^2 + D_{pg,\lambda_2} - D_{pg,\lambda_3})^2}}{3} \tag{12}$$

When the triplet spacing is minimized for a solution set (ideally reaching a value of zero) the D_{pg} and σ_g values are returned for that species. Though not included as a factor in the algorithm, it is of interest to note the relative ordering of the α_{sp} values ($\alpha_{sp,red} > \alpha_{sp,green} > \alpha_{sp,blue}$) from the MLR provide insight into which solution set will likely converge, as the ordering of the wavelengths inverts near the center of the distribution.

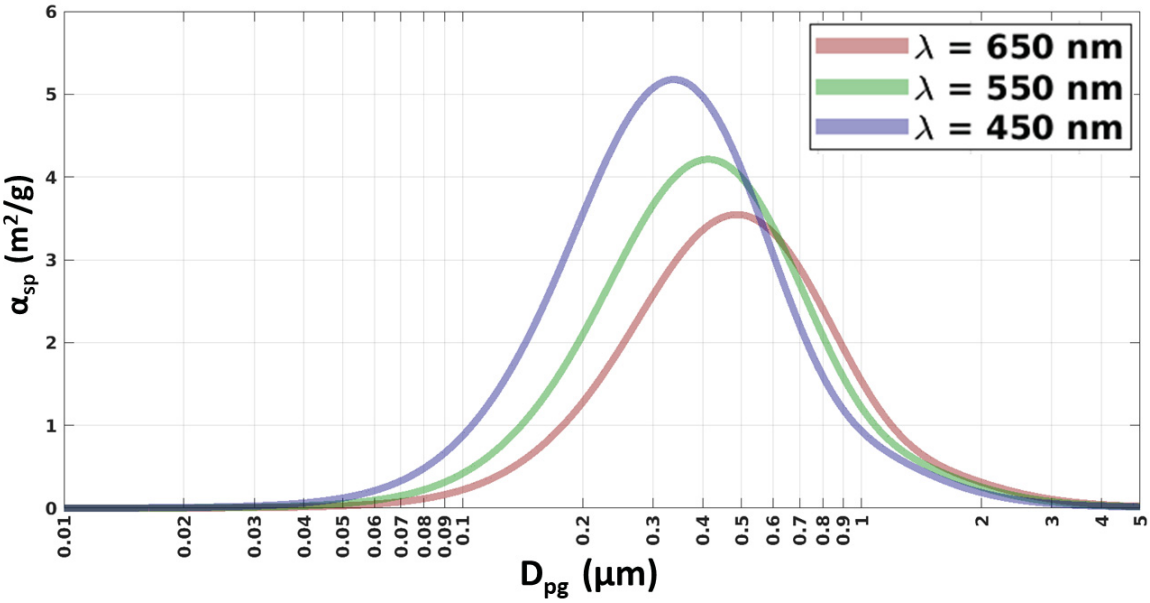

Figure 4: α_{sp} as a function of D_{pg} for a distribution σ_g value of 1.7. At a given D_{pg} value, the 3 α_{sp} values diverge at smaller values and converge for larger values of D_{pg}.

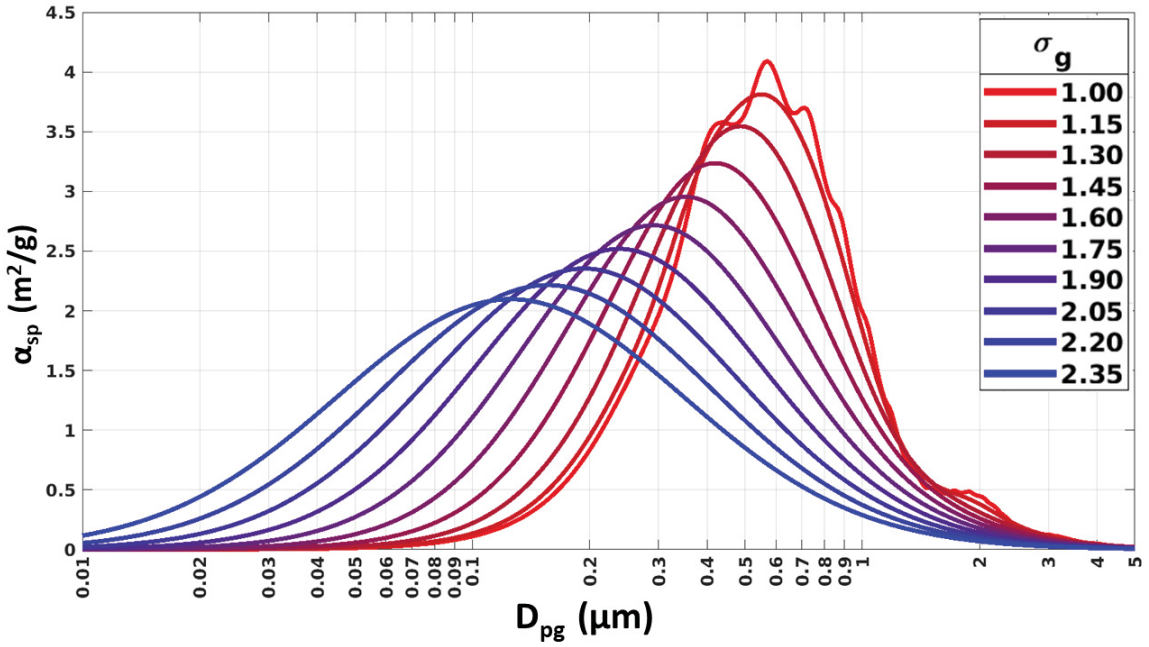

Figure 5: The multiple theoretical α_{sp} curves that exist for a compound at a single incident wavelength, for 10 values of σ_g.

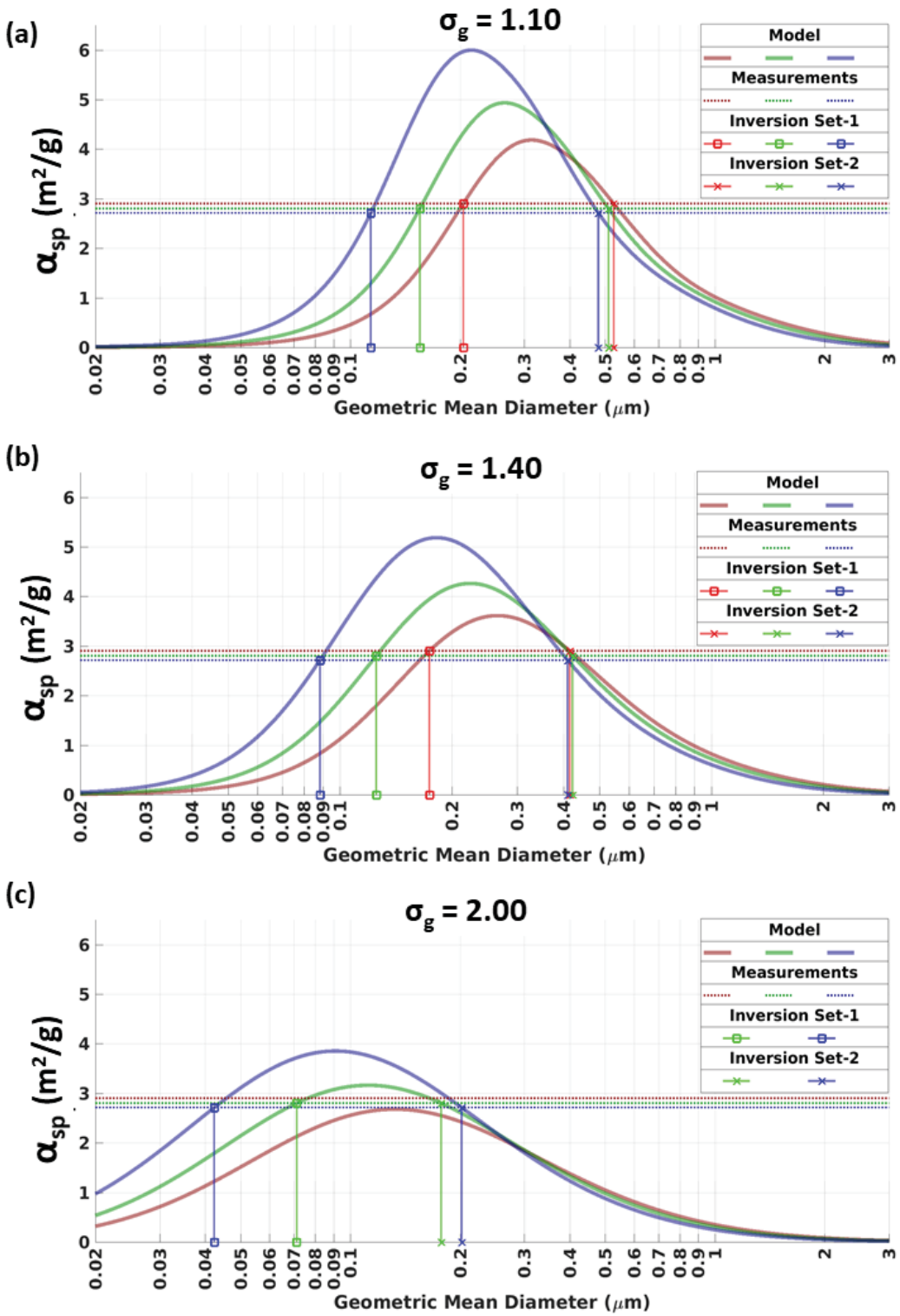

Figure 6: Inversion results for Black Carbon D_{pg} at σ_g values of 1.10, 1.40, and 2.00. Red lines correspond to 650 nm, green lines to 550 nm, and blue lines to 450 nm values.

NEPHELOMETER TRUNCATION

To account for the angular illumination function non-idealities which lead to nephelometer truncation, as set of truncation correction factors is developed. Truncation correction factors are calculated as per the methods of Moosmuller et al [21]. Scattering intensity, given by $|P(\theta)|^2$, and scattering intensity is integrated in the angular exclusion regions and divided by total scattering intensity as in equation 13.

$$\psi_\lambda = \frac{\int_{0^\circ}^{7^\circ} |P(\theta)|^2 d\theta + \int_{173^\circ}^{180^\circ} |P(\theta)|^2 d\theta}{\int_{0^\circ}^{180^\circ} |P(\theta)|^2 d\theta} \tag{13}$$

The truncation factors (ψ_λ) for three sizes of particles is depicted in figure 7. At small size-parameter values ($X = \frac{2\pi r}{\lambda}$), both forward and backward truncation are nearly equal and relatively small (5 % of total scattering). At the larger size-parameter of $X = 10$, scattering is heavily forward biased, which results in a notable asymmetry between back-scatter correction (0.40 % of scatter) and forward-scatter correction (58.61 % of scatter). A corollary of the large truncation factors observed for large size-parameters is that the IN1002 instrument is insensitive to the measurement of scattering at large size-parameters.

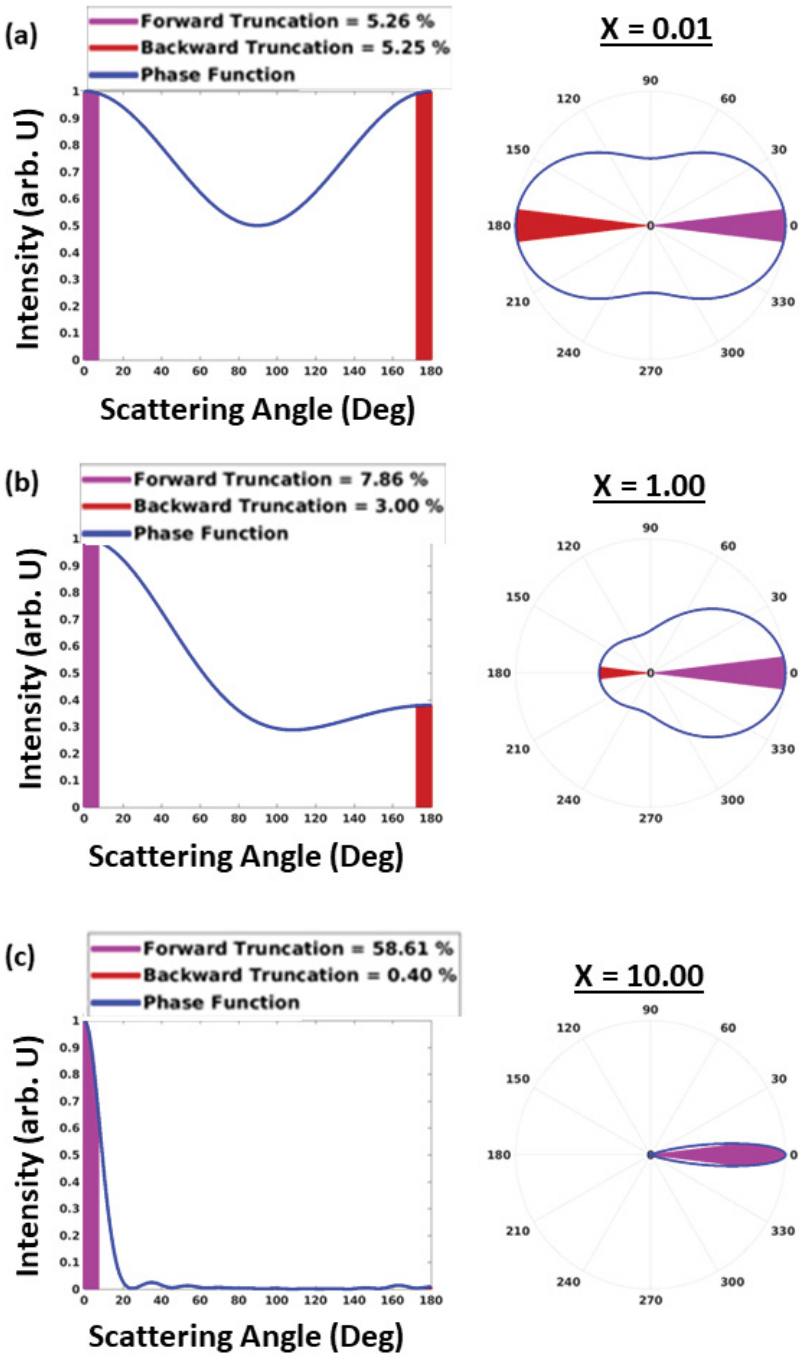

Figure 7: Truncation correction factors at three size parameter values. Plotted in Cartesian coordinated on the left and polar coordinates in the right plots. X indicates the size-parameter depicted in each set of figures.

INVERSION ERROR

The uncertainty in the inverted D_{pg} values is determined from the standard deviation in the α_{sp} values for each species calculated in the MLR. The uncertainty provides a 1-σ confidence-interval around the

average α_{sp} for a species that are applied to the theoretical α_{sp} curves for the σ_g identified by convergence in the previous step. The upper and lower limits of the one standard deviation confidence bars when inverted using intersections with the theoretical α_{sp} curves provides the range of D_{pg} values due to uncertainty in the α_{sp} values from the MLR. The steepness of the α_{sp} vs D_{pg} curves leads to relatively small error surrounding an inverted D_{pg} value.

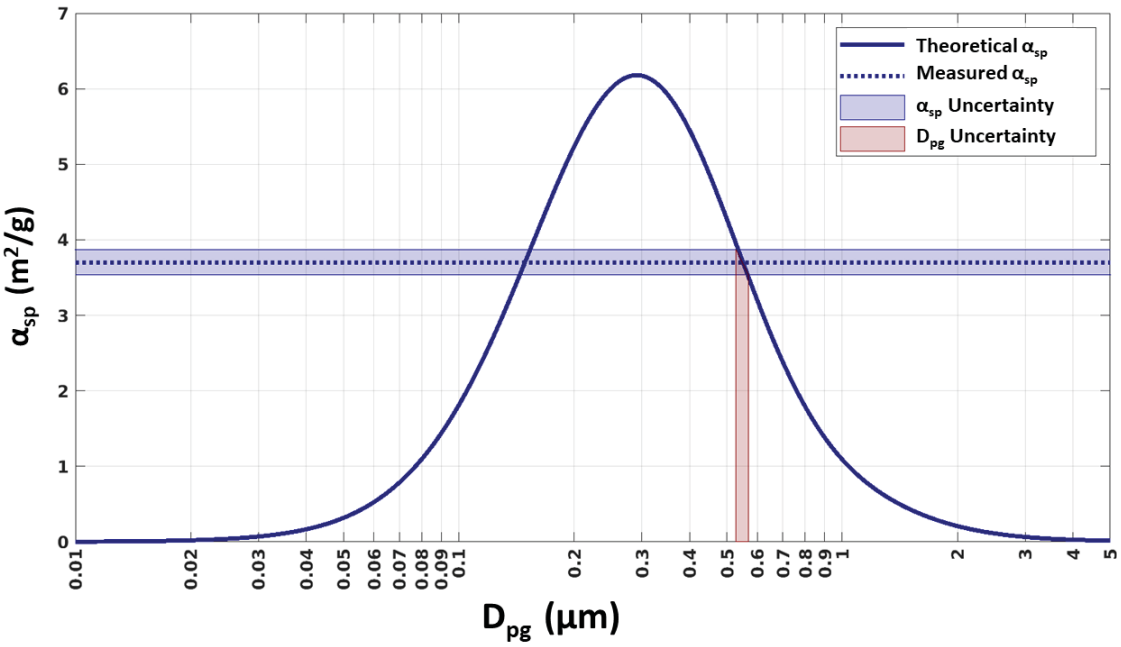

Figure 8: Error in D_{pg} associated with inversion through a theoretical α_{sp} vs D_{pg} curve and the α_{sp} value and its uncertainty determined for a species from a MLR.

CHAPTER 3 RESULTS

MEASUREMENT RESULTS

The average chemical composition results obtained from the five measurement sites that were established for this study are depicted in figure 9. The results are based upon the chemical analysis of 48 filters across all sampling sites. The filter break-down for each site was not evenly distributed due to differing dates that the sites initiated sampling as well as instrument downtime due to maintenance that modified the sampling schedules of each of the sites to differing degrees. The largest number of filters was analyzed from the Sherbrooke site (27), followed by Halifax (14), then Downsview (13), Lethbridge (11), and finally Kelowna (2). The total number of filters analyzed across all sites is thus 48, representing 432 days of $PM_{2.5}$ sampling. The five chemical components and the total $PM_{2.5}$ concentration show pronounced heterogeneity across sites, with the high $PM_{2.5}$ concentrations in Lethbridge being driven by the elevated concentrations of organics (POM) and to a lesser degree SIA. The only site with appreciable levels of sea-salt was the coastally located Halifax sampling site, which is in line with an ocean-emission source and relatively short atmospheric transport distances of this species [28]. The elevated concentrations of black carbon in Lethbridge combined with the elevated POM and total $PM_{2.5}$ could point toward forest-fires as a dominant source in the $PM_{2.5}$ of this region of Canada.

Figure 9 presents the results of $PM_{2.5}$ fractional composition, total $PM_{2.5}$ mass concentration, b_{sp} and finally α_{sp}, broken down by site. The average α_{sp} values of all sites are the same within error. Lethbridge presents as a notable exception in terms of the variance of the measured properties. The large variability in both $PM_{2.5}$ and b_{sp} is likely attributable to local biomass burning during the forest fire season of Western Canada causing elevated $PM_{2.5}$ concentrations.

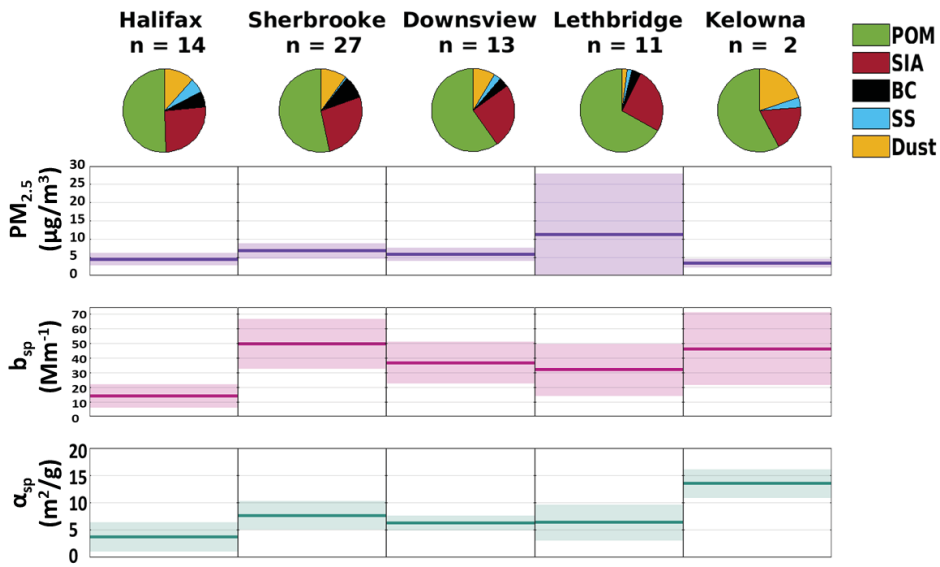

Figure 9: Average measurement results from the five measurement sites of this study. Shaded area represents 1-σ variance about the mean.

COMPARISON WITH GEOS-CHEM

A main goal of this research is to produce refined information to improve the simulation of optical aerosol interactions in the chemical transport model GEOS-Chem. It is thus relevant to compared simulated $PM_{2.5}$ composition as well as simulated optical properties such as α_{sp} and b_{sp} to those values found in this study as well as in other measurement networks. The measurement networks used for this comparison are 158 sites from IMPROVE active between 2000-2016 and 36 measurement sites from the NAPS network active between 2015-2017. Only a subset of 13 of the IMPROVE sites had concurrent scattering measurements along with filter-based sampling measurements and no NAPS sites have collocated scattering measurements reported, leading to the reduced number of comparison sites in panels *g* and *h* of figure 10. A GEOS-Chem simulation nested over North America with 0.5x0.25° resolution and 2014 GFED (Global Fire Emission Database) emission inventories is used for comparison with optical properties parameterized by Latimer et al for SIA and POM and GADS for BC, Sea-salt and Dust [16, 27]. Time periods are not strictly overlapping for the measurement and model data-sets, so comparisons are done using one year average values for the simulation, and full sampling time-period average for the measurements, which varies from 1-10 years depending upon the site. Total $PM_{2.5}$

concentration is shown in panel (*a*) of figure 10 where the MAPLE measurements are consistent with both other networks as well as simulated $PM_{2.5}$ except for one notable outlier that comes from the Lethbridge site in Western Canada. The high $PM_{2.5}$ values seen in Lethbridge in panel *a* are partially explained by the elevated POM and BC at this site in panels *b* and *d* compared to model; the elevation of these two components points toward forest fires that are not represented in the 2014 GFED inventory used in the simulation [29]. Model over-estimation of SIA is more pronounced at the norther NAPS and MAPLE sites than at the IMPROVE sites. This bias is attributed to the well-documented nitrate aerosol over-estimation problem in GEOS-Chem [30]. Notable differences between the overestimate in the Canadian networks (MAPLE and NAPS) and the US based network IMPROVE may be due to continental temperature gradients influencing simulated nitrate dry-deposition [31]. Sea-salt is low at all sites beside Coastal locations, which produces good agreement between all networks and the model. Crustal material or Dust, in panel *f* shows very high model underestimation at both NAPS and MAPLE sites, with model biases lower than 0.10 and moderate correlations of 0.36 and 0.52, respectively. MAPLE sites show low bias versus model for $b_{sp,550}$, though there is low correlation (R^2=0.13). Model values from IMPROVE site locations for $b_{sp,550}$ are biased high (bias = 1.70) with low correlation (R^2=0.18). The α_{sp} values from the IMPROVE sites are lower than the values from the MAPLE sites, however GEOS-Chem significantly over-estimates the α_{sp} values at the IMPROVE sites (bias = 3.22) compared to the closer agreement found between model and measurement from the MAPLE sites (bias=1.15).

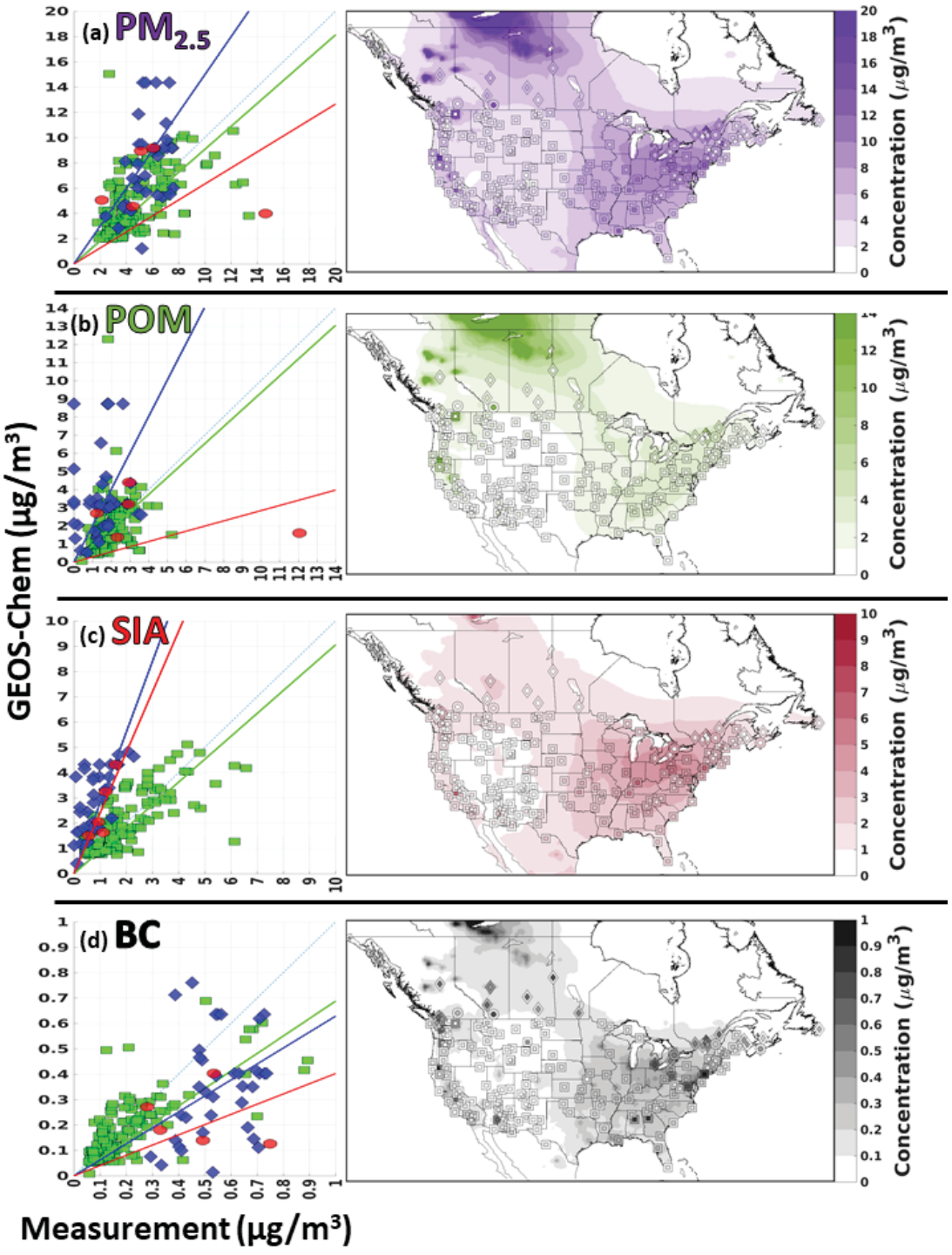
(a) PM2.5
(b) POM
(c) SIA
(d) BC
GEOS-Chem (µg/m³)
Measurement (µg/m³)
Concentration (µg/m³)

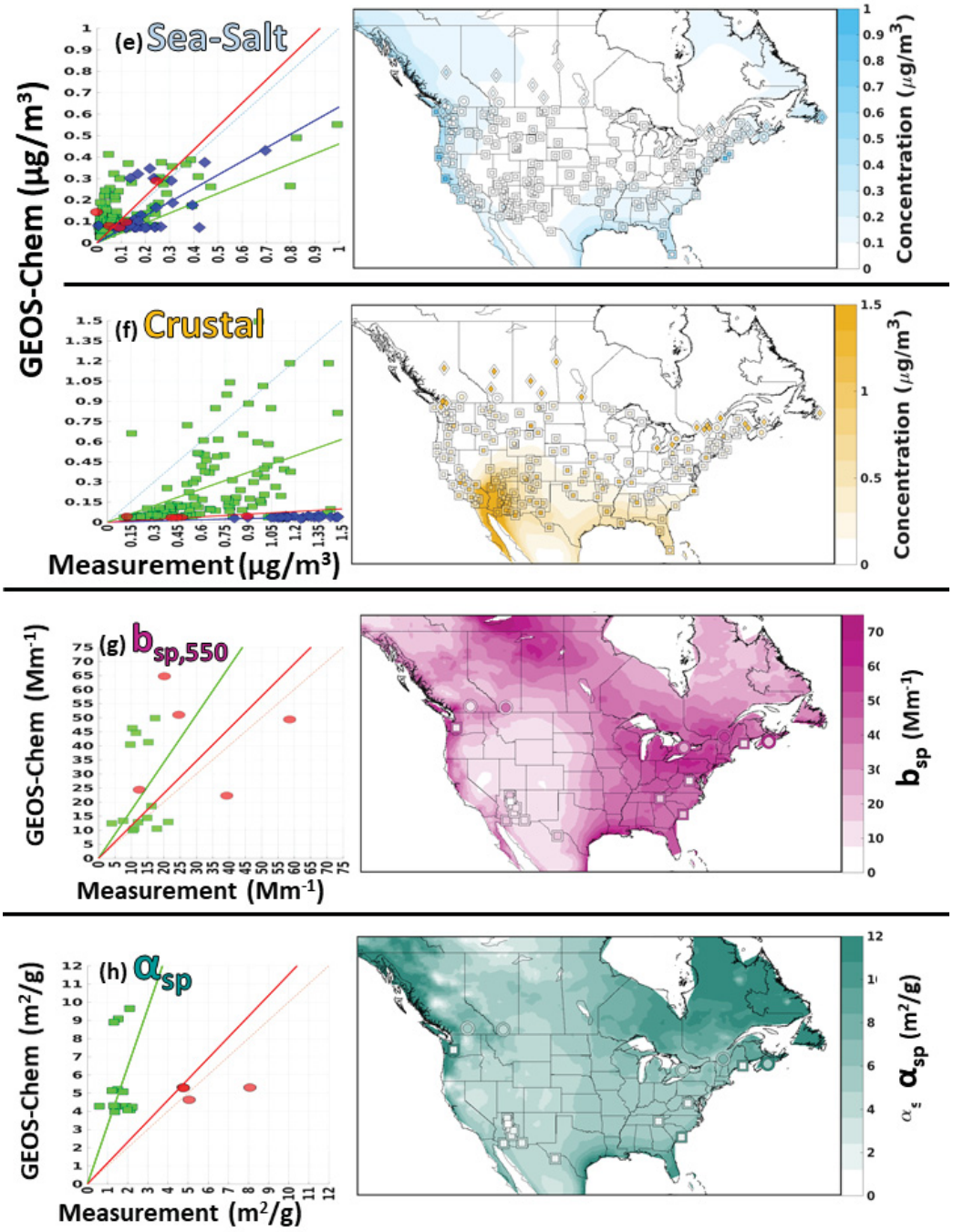

Figure 10: Comparison of average simulated $PM_{2.5}$, POM, SIA, BC, Sea-salt, Dust, $b_{p,550nm}$, and α_{sp} compared to average measured values from three networks: IMPROVE (Square symbols), NAPS (diamond symbols), MAPLE (circle symbols). Bias and correlation values between measurement and model are inset for each network on each plot. Points in the scatter plots represent the average values from individual measurement sites. Insets of symbols represents measurement values and outer-rings of symbols represents collocated model values.

Property	Fit Statistic	IMPROVE	NAPS	MAPLE
$PM_{2.5}$	R^2	0.48	0.10	0.37
	bias	0.91	1.50	0.63
POM	R^2	0.26	0.14	0.37
	bias	0.93	2.01	0.28
SIA	R^2	0.68	0.61	0.68
	bias	0.91	2.80	2.40
BC	R^2	0.68	0.14	0.22
	bias	0.69	0.63	0.40
Sea-Salt	R^2	0.63	0.47	0.65
	bias	0.46	0.63	1.09
Crustal	R^2	0.36	0.33	0.52
	bias	0.41	0.03	0.07
b_{sp}	R^2	0.18	-	0.13
	bias	1.70	-	1.15
α_{sp}	R^2	3.22	-	0.26
	bias	0.26	-	1.15

Table 1: Linear regression statistics from scatter plots presented in figure 10. Bias values are presented for Model/Measurement

MULTIPLE LINEAR REGRESSION

Here we examine the results of the multiple linear regression that was performed on the chemical and optical measurements obtained in this study. Specifically, the MLR was performed on the data-set depicted in figure 11. The MLR provides an estimate of the α_{sp} of each of the 5 aerosols components investigated in this study for each of the three wavelengths of analysis from the Nephelometer. As seen in figure 12, for all species the α_{sp} values follow the trend of being correlated with the wavelength of analysis. The α_{sp} values are larger for the larger wavelength than for the smaller wavelengths. As discussed in the methods section regarding the development of the SYRUP algorithm, this ordering of the α_{sp} values based upon wavelength provides valuable insight into the likely size-region that the SYRUP algorithm will determine for these species, corresponding to solution set two from figure 12. In the

right-most panel of figure 12 the average α_{sp} values at a wavelength of 550 nm compiled from the 60 studies on α_{sp} as reported by Hand et al are shown in comparison to the α_{sp} values obtained from the MLR in this study [13]. The mass scattering efficiency of Black Carbon is taken from a the series of short-term studies performed by Holder et al of forest fires in the United States [32]. Holder's BC α_{sp} values are significantly larger than those found in this study. This may be due in part to differences in source proximity compared to Holder. This would influence aerosol aging effects, which has been noted by Lowenthal et al to have a large effect on size-distribution and measured optical properties [33]. The close agreement of the measurement results for the other four components of $PM_{2.5}$ with the ranges found in literature provides promising evidence for the veracity and robustness of both the compositional and optical measurements as well as the stability of the MLR method at discerning the α_{sp} values of the individual species. The large variance associated with the MLR results for sea-salt, black carbon and to a lesser extent dust are likely an indication as described by Vasconcales of the correlation of these species with more than one size-mode (accumulation and coarse-mode), as the two size-modes will possess different α_{sp} values for a single-species [17].

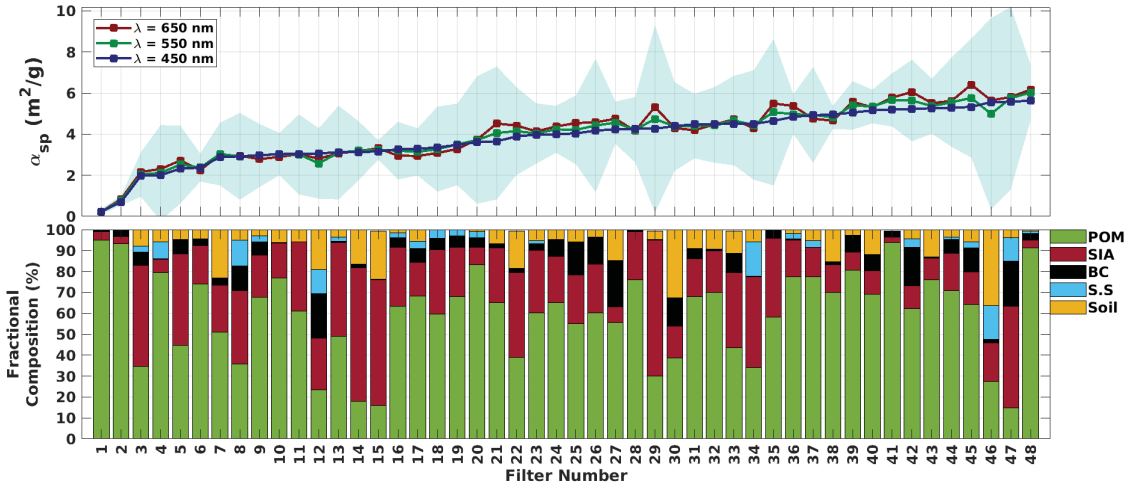

Figure 11: Fractional Composition and α_{sp} of all sampled filters. Filters ordered from lowest to highest α_{sp} values, no sampling trend is implied.

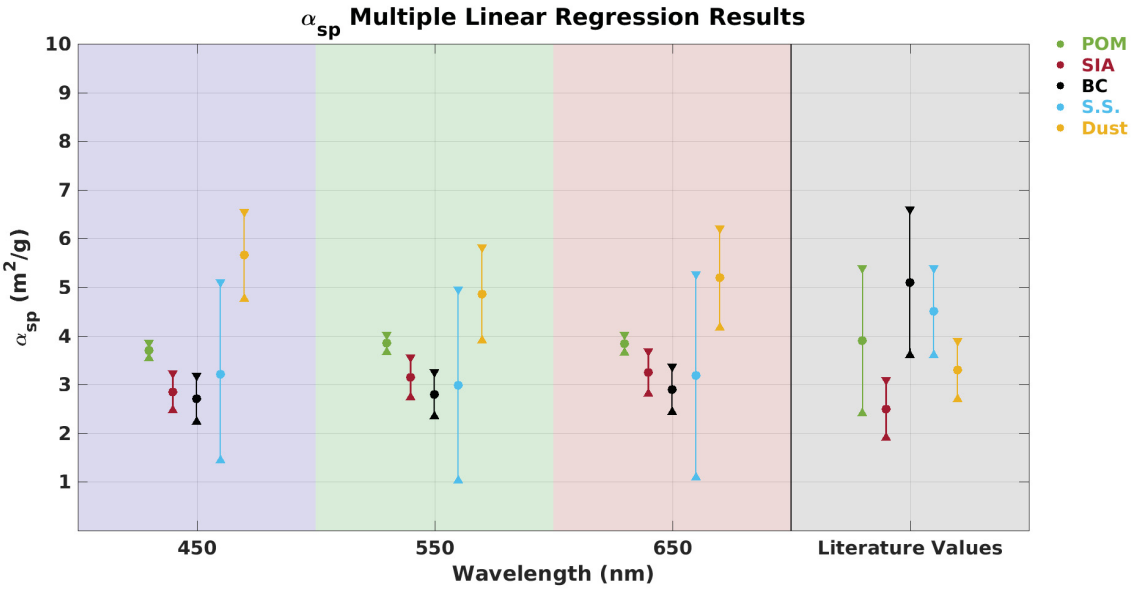

Figure 12: Component based breakdown of α_{sp} at three wavelengths of Nephelometer measurement, as well as literature values for each

SIZE-INVERSION RESULTS

The SYRUP algorithm was performed on the α_{sp} values determined by the MLR for of each species presented in figure 12. Unique size-distribution parameters were returned for all five species of aerosol. As described in the methodology of the SYRUP algorithm, the solutions to the size-distribution parameters are based upon the convergence of the three-wavelengths of analysis within a given solution set on a D_{pg} value for a single value of σ_g. Put in another way, the algorithm searches for the minimization in triplet-spacing within a solution set across D_{pg} and σ_g space. This convergence of the answers for a set and therefore the minimization of triplet-spacing for that solution-set is depicted in panel (b) of figure 6. The significance of the termination of the solution sets at specific values of σ_g is that for σ_g values greater than this, there ceases to be intersections between the measured α_{sp} values and the theoretical α_{sp} curves for all three wavelengths, hence a solution cannot exist given the requirements placed on the minimization of triplet spacing. The numerical results are presented in full, for each wavelength, including the errors associated with the inversion in table 2. The large error associated with the inversion

for sea-salt is likely due to this species being present in appreciable quantities only in Halifax. There is therefore little certainly placed in the inversion results for this species.

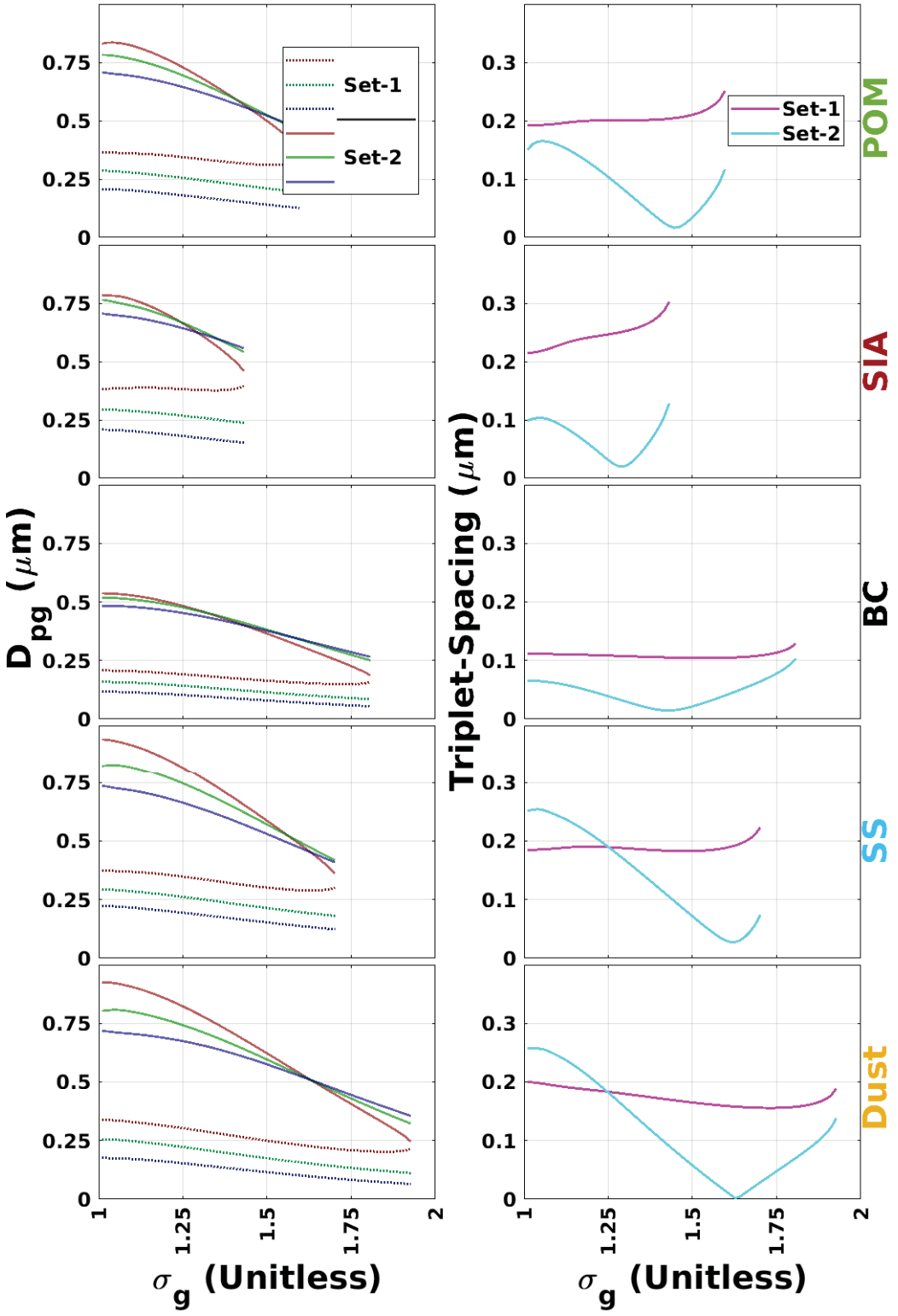

Figure 13: Solution set-1 refers to the solutions on the left side of the α_{sp}maximum from Figure 6, while solution set-2 refers to the right hand solutions. The top panel shows the D_{pg} solutions for each wavelength at a range of σ_g values. The bottom panel depicts the average distance between any two colour pairs for a given solution. When this spacing is minimized, this is taken to mean that the most accurate $_g$ value has been found, as has the D_{pg} value

Aerosol	Wavelength	D_{pg}	ST.DEV	R_{eff}	ST.DEV	σ_g
	(nm)	μm	μm	μm	μm	(Unitless)
POM	450	0.55	0.08	0.34	0.04	1.45
	550	0.56	0.08	0.35	0.04	
	650	0.56	0.06	0.35	0.03	
SIA	450	0.62	0.04	0.34	0.02	1.30
	550	0.64	0.08	0.35	0.04	
	650	0.62	0.12	0.34	0.06	
BC	450	0.41	0.08	0.27	0.04	1.40
	550	0.42	0.08	0.28	0.04	
	650	0.42	0.12	0.28	0.06	
Sea-Salt	450	0.46	0.72	0.33	0.35	1.61
	550	0.47	0.68	0.34	0.34	
	650	0.48	0.70	0.33	0.35	
Dust	450	0.51	0.10	0.36	0.05	1.63
	550	0.51	0.10	0.36	0.05	
	650	0.51	0.20	0.37	0.10	

Table 2: Summary of the inversion results from the SYRUP algorithm for each of the five species investigated in this study, reported at each wavelength of inversion.

VALIDATION OF SIZE-INVERSION RESULTS

Presented in table 3, the size-distribution results of the SYRUP algorithm constitute a proposed increase to the sizes of all species compares to the findings of several other studies that have informed the size-distribution values in the GEOS-Chem model in the past. Considering this large increase, it is necessary to provided corroborating evidence to support the proposed increase in the dry-radii for all species. In lieu of collocated size-distribution measurements, the validation of the SYRUP algorithm is performed via comparison with scanning mobility particle sizer (SMPS) measurements conducted in East Trout Lake, Saskatchewan as well as using simulated aerosol sizes from the TOMAS15 aerosol microphysics model. Sangeeta Sharma from Environment and Climate Change Canada (ECCC) performed SMPS analysis in East Trout Lake, SK from 2013 to 2015 as a part of the Canadian Aerosol Baseline Measurement program (CABM) and provided access to the unpublished data for comparison here. The dry effective radii from

this data are presented in figure 14 as monthly averages. The effective radii of the aerosol distributions measured in East Trout Lake bolsters the need to increase the effective radius of the aerosols compared to those previously found in table 3.

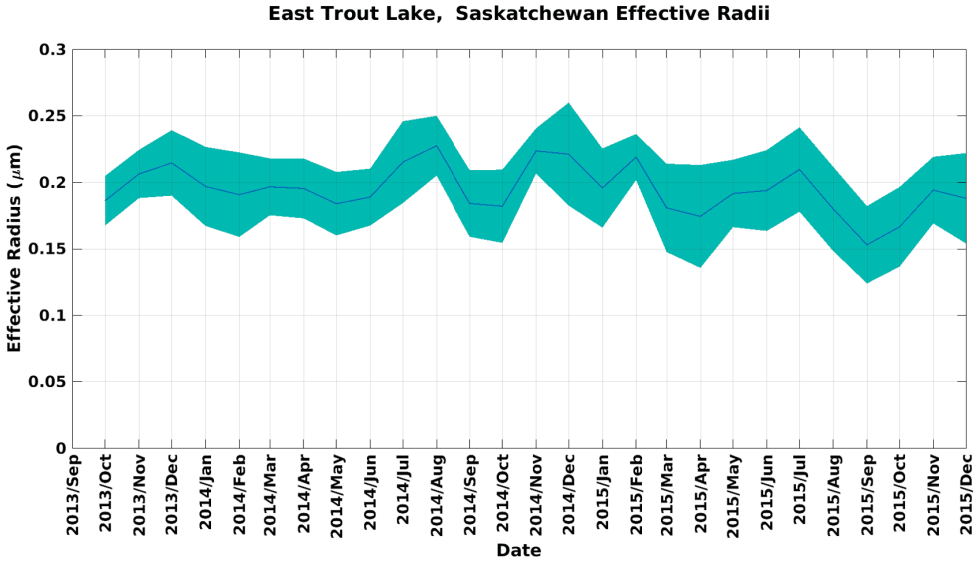

Figure 14: Monthly effective radius values calculated from SMPS measurements. Error-bars represent 1σ

The TOMAS15 aerosol microphysics simulation was conducted using 15 size-bins and was nested over North America with a simulation resolution of 2x2.5 $^\circ$ for 2013-2015. Model results are outputted under dry conditions (RH $= 0\%$). This microphysical model provides motivation for the geographic variation that might be expected in R_{eff} at the 5 measurement sites of this study dispersed across the mid-latitudes of Canada. As the MLR was performed on all sites in aggregate rather than on a site-by-site basis due to data-set size considerations, the R_{eff} values obtained from the results of the SYRUP algorithm provide a single value for all-sites in this study. In figure 15 the same R_{eff} value is overlaid for each site across Canada to aid in comparison of the geographic variation across Canada of this property and the agreement with simulated values that this inversion provides. Greater over-estimation is observed for the R_{eff} values in western Canada, owing to the smaller predicted R_{eff} values in this region by the TOMAS simulation. However, in aggregate, the effective radii suggested by the SYRUP algorithm are in excellent agreement with the effective radii simulated by this model. This helps to bolster the argument for an increase in the effective radii of all species, as suggested by the conclusions of this study.

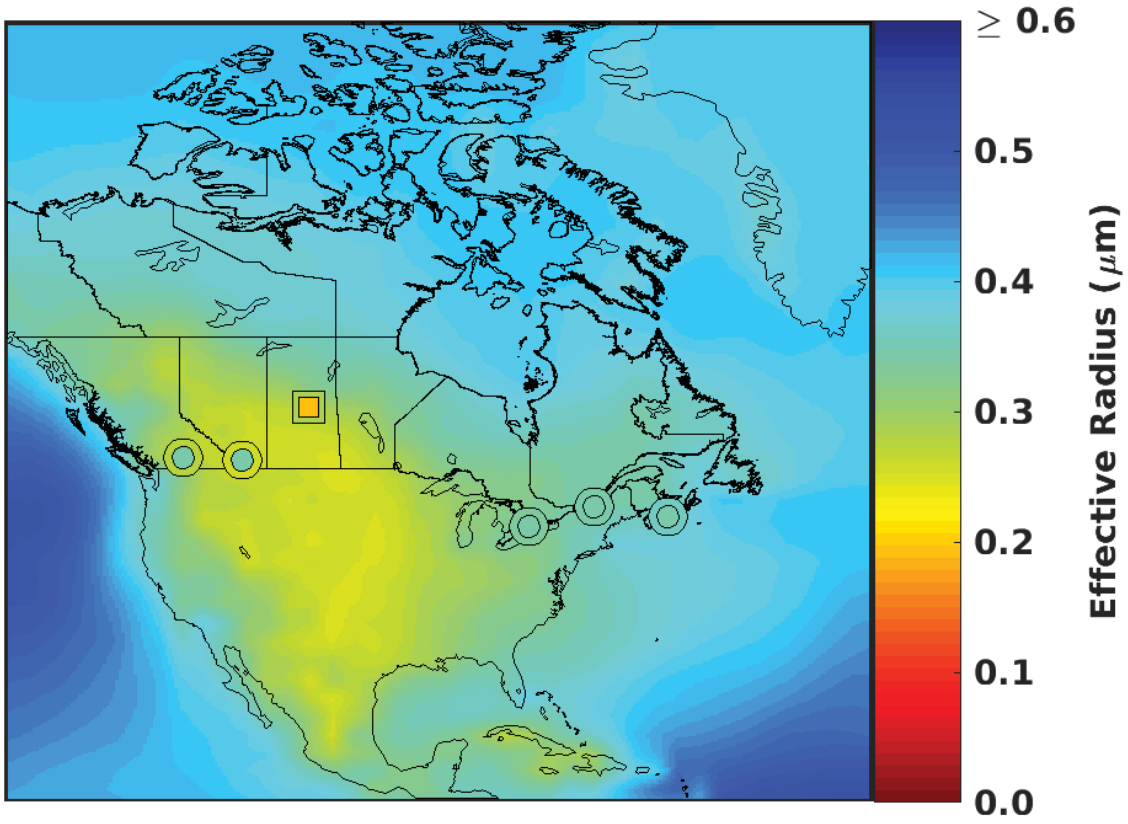

Figure 15: TOMAS average surface-level effective radius over North America compared to the inverted size of POM at MAPLE sites (circles) and East Trout Lake, SK (square). Insets of symbols represents measurement values and outer-rings of symbols represents collocated model values

The in-depth analysis performed by Drury et al has served as one of the key studies informing aerosol size-distribution properties for geochemical transport models in the past [16, 34]. It is thus of particular importance to address the differences between the findings of Drury et al with the results of this study. The basis of the size-distribution data in Drury's study comes from the ICARTT aircraft campaign of 2004. This campaign was conducted between July 6th-August 14th, 2004 in the Eastern United States. An optical particle counter (OPC) is used aboard the aircraft to directly measure total aerosol size-distributions from elevations of 0.3 to 12 km [34]. Size-parameters for each species are determined using the measured total species size-distributions as well as aerosol chemical composition measurements taken simultaneously aboard the aircraft of POM, SIA, Dust, and BC; sea-salt is excluded from this analysis due to its limited concentrations over the mainly continental region of measurements [34]. Size-parameters for each species are determined by varying the D_{pg} and σ_g values for each species to improve

agreement with the OPC measurements, with total mass-concentration for each species constrained by measurement [34]. It is unclear from the methodologies described by Drury et al how the vertical extent of their measurements are used in the determination of single values for the particle size-parameters that are reported independent of elevation. There appears to be relatively little variation in the total distribution D_{pg} values and thus the method of vertical integration (entire vertical extent vs bottom 1 km only) is likely to be only a minor factor in the calculation of the final size-parameters. It is of interest to note that the TOMAS model predicts much greater vertical variation in the particle diameter than was found by Drury et al as can be seen in figure 16. Perhaps the main factor driving differences between the findings of Drury et al and the findings of this study is the limited temporal extent of the ICARTT measurements upon which the analysis of Drury et al is based not capturing the seasonal variation in the particle size-distributions. The seasonal variation predicted by the TOMAS model are given in figure 17, which corroborate the findings of this study with those of Drury being likely due to the differences in the measurements time-frame of the respective studies.

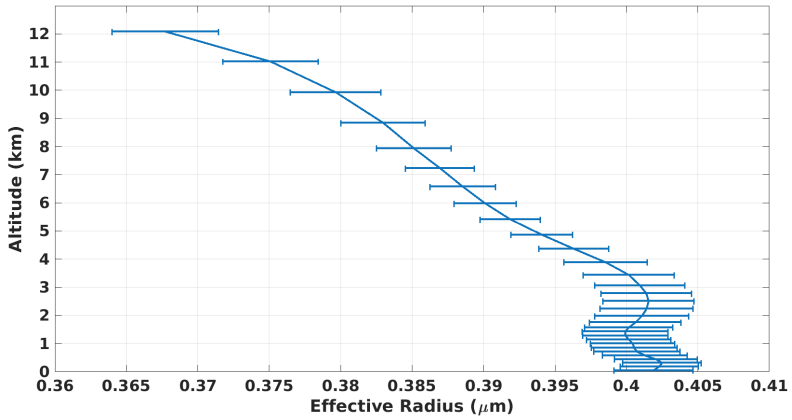

Figure 16: Average TOMAS vertical trend in effective radius from 0 to 12 km altitude. Horizontal error-bars represent 1-σ variance about the mean.

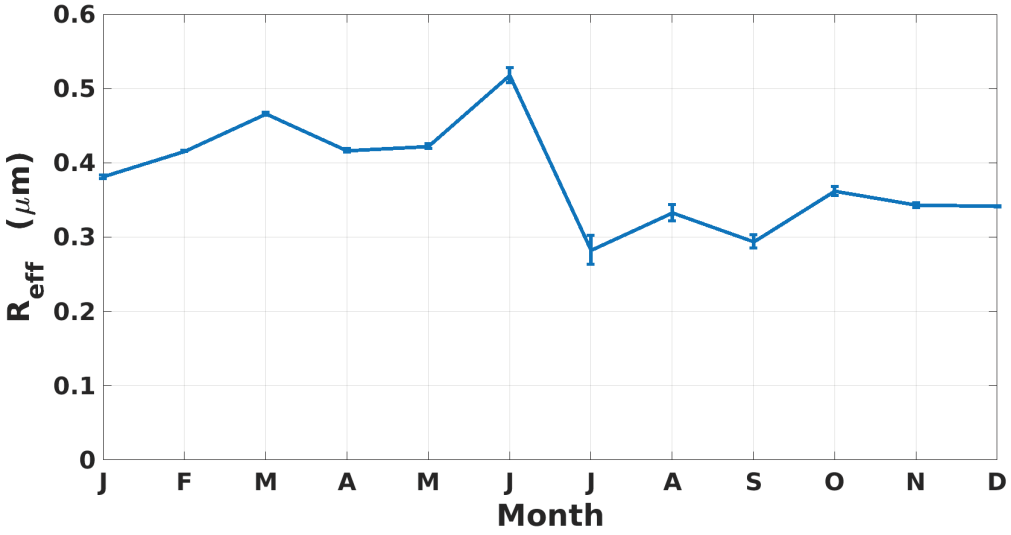

Figure 17: Monthly effective radius values from the TOMAS model calculated over the spatial measurement domain of the ICARTT study. Error-bars represent 1σ

The differences between the findings of Latimer et al and this study are attributed to the methodological differences in the approaches to solving for size-distributions from α_{sp} measurements [16]. The simplifications employed in the Latimer study were due in part to the previously published findings of Drury et al possibly motivating the refinement of the particles sizes to only those within range of what had previously been reported. It is therefore not viewed as corroborating evidence that Drury and Latimer find similar size-distribution parameters.

Aerosol	Property	Units	GADS [27]	Drury et al [34]	Latimer et al [16]	This Study
POM	D_{pg}	(μm)	0.05	0.17	0.13	0.56
	σ_g	(Unitless)	2.24	1.60	1.60	1.45
	D_{eff}	(μm)	0.13	0.30	0.23	0.79
	α_{sp}	(m^2/g)	4.33	5.19	3.99	4.40
SIA	D_{pg}	(μm)	0.20	0.20	0.13	0.62
	σ_g	(Unitless)	2.00	1.60	1.60	1.3
	D_{eff}	(μm)	0.66	0.35	0.20	0.68
	α_{sp}	(m^2/g)	3.32	5.67	3.05	4.36
BC	D_{pg}	(μm)	0.02	0.04	-	0.42
	σ_g	(Unitless)	2.00	1.60	-	1.40
	D_{eff}	(μm)	0.06	0.04	-	0.55
	α_{sp}	(m^2/g)	4.86	4.50	-	4.27
Sea-Salt	D_{pg}	(μm)	0.17	-	-	0.46
	σ_g	(Unitless)	1.50	-	-	1.61
	D_{eff}	(μm)	0.258	-	-	0.81
	α_{sp}	(m^2/g)	2.38	-	-	2.61
Dust	D_{pg}	(μm)	0.30	0.11	-	0.51
	σ_g	(Unitless)	2.20	2.20	-	1.63
	D_{eff}	(μm)	0.59	0.41	-	0.65
	α_{sp}	(m^2/g)	4.34	4.25	-	3.46

Table 3: Comparison of aerosol size-distribution properties that have been reported in the literature previously for dry aerosol properties. The α_{sp}values are all reported at an RH $= 0$, and at an incident wavelength of 550 nm.

CHAPTER 4 CONCLUSIONS

This study deployed five measurement sites across Canada (Halifax, Sherbrooke, Downsview, Lethbridge, and Kelowna) between 2017-2019 equipped with filter sampling stations to collect and analyze the physical and chemical properties of $PM_{2.5}$ as well as with a nephelometer to measure ambient scattering at three wavelengths. Correction factors are applied to account for increases in ambient scattering due to water uptake compared to dry-aerosol mass. Reconstruction of $PM_{2.5}$ composition into 5 chemical components (POM, SIA, BC, SS, and Dust). A multiple linear regression is used to determine the mass scattering efficiency of five chemical components of $PM_{2.5}$. The SYRUP algorithm is developed to invert the measured α_{sp} values using Mie scattering theory, and applying truncation correction factors to adjust modeled scattering values to fit those measured by a nephelometer. The SYRUP algorithm returns geometric mean diameter values of 0.56, 0.62, 0.42, 0.46, and 0.51 μm for POM, SIA, BC, SS, and Dust, respectively. The variance (σ_g) of the lognormal distributions determined for these species is 1.45, 1.30, 1.40, 1.61, and 1.63, for the same species as above. Owing to only a small subset of samples from Halifax having sea-salt present, the reliability of these number should be taken with a grain of salt as well. The increases in dry particle sizes that are proposed above compared to smaller values that have been previously used in CTM's is validated using SMPS measurements from ECCC's CABM East Trout Lake site, along with the comparison to particle sizes predicted using the TOMAS15 aerosol microphysics model.

BIBLIOGRAPHY

[1] Aaron van Donkelaar et al. "Global Estimates of Fine Particulate Matter using a Combined Geophysical-Statistical Method with Information from Satellites, Models, and Monitors". In: *Environmental Science & Technology* 50.7 (Apr. 2016), pp. 3762–3772. ISSN: 0013-936X. DOI: 10.1021/acs.est.5b05833. URL: http://pubs.acs.org/doi/10.1021/acs.est.5b05833.

[2] O. Dubovik et al. "Statistically optimized inversion algorithm for enhanced retrieval of aerosol properties from spectral multi-angle polarimetric satellite observations". In: *Atmospheric Measurement Techniques* 4.5 (May 2011), pp. 975–1018. ISSN: 1867-8548. DOI: 10.5194/amt-4-975-2011. URL: http://www.atmos-meas-tech.net/4/975/2011/.

[3] O. Dubovik et al. "Accuracy assessments of aerosol optical properties retrieved from Aerosol Robotic Network (AERONET) Sun and sky radiance measurements". In: *Journal of Geophysical Research: Atmospheres* 105.D8 (Apr. 2000), pp. 9791–9806. ISSN: 01480227. DOI: 10.1029/2000JD900040. URL: http://doi.wiley.com/10.1029/2000JD900040.

[4] Oleg Dubovik and Michael D. King. "A flexible inversion algorithm for retrieval of aerosol optical properties from Sun and sky radiance measurements". In: *Journal of Geophysical Research: Atmospheres* 105.D16 (Aug. 2000), pp. 20673–20696. ISSN: 01480227. DOI: 10.1029/2000JD900282. URL: http://doi.wiley.com/10.1029/2000JD900282.

[5] V Feigin et al. "Global, Regional, and National Burden of Epilepsy, 1990-2016: A Systematic Analysis for the Global Burden of Disease Study 2016". In: *The Lancet Neurology* 18.4 (2019), pp. 357–375.

[6] Ranu Gadi, Sudhir Kumar Sharma, Tuhin Kumar Mandal, et al. "Source apportionment and health risk assessment of organic constituents in fine ambient aerosols (PM2. 5): A complete year study over National Capital Region of India". In: *Chemosphere* 221 (2019), pp. 583–596.

[7] Jongeun Rhee et al. "Impact of Long-Term Exposures to Ambient PM2. 5 and Ozone on Acute Respiratory Distress Syndrome (ARDS) Risk for Older Adults in the United States". In: *Chest* (2019).

[8] Liji M David et al. "Premature mortality due to PM2. 5 over India: Effect of atmospheric transport and anthropogenic emissions". In: *GeoHealth* 3.1 (2019), pp. 2–10.

[9] Judith C. Chow et al. "Comparability between PM2.5 and Particle Light Scattering Measurements". In: *Environmental Monitoring and Assessment* 79.1 (Oct. 2002), pp. 29–45. ISSN: 1573-2959. DOI: 10.1023/A:1020047307117. URL: https://doi.org/10.1023/A:1020047307117.

[10] Karl J. Siebert. "Relationship of Particle Size to Light Scattering". In: *Journal of the American Society of Brewing Chemists* 58.3 (2000), pp. 97–100. DOI: 10.1094/ASBCJ-58-0097. eprint: https://doi.org/10.1094/ASBCJ-58-0097. URL: https://doi.org/10.1094/ASBCJ-58-0097.

[11] Lester G. Telser, J. Aitchison, and J. A. C. Brown. "The Lognormal Distribution". In: *Journal of Farm Economics* 41.1 (Feb. 1959), p. 161. ISSN: 10711031. DOI: 10.2307/1235218. URL: https://academic.oup.com/ajae/article-lookup/doi/10.2307/1235218.

[12] James E. Hansen and Larry D. Travis. "Light scattering in planetary atmospheres". In: *Space Science Reviews* 16.4 (Oct. 1974), pp. 527–610. ISSN: 0038-6308. DOI: 10.1007/BF00168069. URL: http://link.springer.com/10.1007/BF00168069.

[13] J L Hand and W C Malm. "Review of aerosol mass scattering efficiencies from ground-based measurements since 1990". In: *J. Geophys. Res* 112 (2007), p. 16203. DOI: 10.1029/2007JD008484. URL: https://agupubs.onlinelibrary.wiley.com/doi/pdf/10.1029/2007JD008484.

[14] PK Quinn et al. "Aerosol optical properties measured on board the Ronald H. Brown during ACE-Asia as a function of aerosol chemical composition and source region". In: *Journal of Geophysical Research: Atmospheres* 109.D19 (2004).

[15] JL Hand et al. "Aerosol size distributions and visibility estimates during the Big Bend regional aerosol and visibility observational (BRAVO) study". In: *Atmospheric Environment* 36.32 (2002), pp. 5043–5055.

[16] R. N. C. Latimer and R. V. Martin. "Interpretation of measured aerosol mass scattering efficiency over North America using a chemical transport model". In: *Atmospheric Chemistry and Physics* 19.4 (2019), pp. 2635–2653. DOI: 10.5194/acp-19-2635-2019. URL: https://www.atmos-chem-phys.net/19/2635/2019/.

[17] LA de P Vasconcelos et al. "A closure study of extinction apportionment by multiple regression". In: *Atmospheric Environment* 35.1 (2001), pp. 151–158.

[18] G. Snider et al. "SPARTAN: a global network to evaluate and enhance satellite-based estimates of ground-level particulate matter for global health applications". In: *Atmospheric Measurement Techniques* 8.1 (Jan. 2015), pp. 505–521. ISSN: 1867-8548. DOI: 10.5194/amt-8-505-2015. URL: http://www.atmos-meas-tech.net/8/505/2015/.

[19] XH Hilda Huang et al. "Characterization of PM2. 5 major components and source investigation in suburban Hong Kong: a one year monitoring study". In: *Aerosol Air Qual. Res* 14.1 (2014), pp. 237–250.

[20] M D Petters and S M Kreidenweis. *Atmospheric Chemistry and Physics A single parameter representation of hygroscopic growth and cloud condensation nucleus activity*. Tech. rep. 1961. URL: www.atmos-chem-phys.net/7/1961/2007/.

[21] Hans Moosmüller and W Patrick Arnott. "Angular truncation errors in integrating nephelometry". In: (2003). DOI: 10.1063/1.1581355. URL: http://ojps.aip.org/rsio/rsicr.jsp.

[22] Theodore L. Anderson and John A. Ogren. "Determining Aerosol Radiative Properties Using the TSI 3563 Integrating Nephelometer". In: *Aerosol Science and Technology* 29.1 (Jan. 1998), pp. 57–

69. ISSN: 0278-6826. DOI: 10.1080/02786829808965551. URL: http://www.tandfonline.com/doi/abs/10.1080/02786829808965551.

[23] George M Hidy, Volker Mohnen, and Charles L Blanchard. "Tropospheric aerosols: Size-differentiated chemistry and large-scale spatial distributions". In: *Journal of the Air & Waste Management Association* 63.4 (2013), pp. 377–404.

[24] W Reed Espinosa et al. "Retrievals of aerosol optical and microphysical properties from Imaging Polar Nephelometer scattering measurements". In: *Atmospheric Measurement Techniques* 10.3 (2017), pp. 811–824.

[25] Judith C. Chow et al. "Mass reconstruction methods for PM2.5: a review". In: *Air Quality, Atmosphere & Health* 8.3 (June 2015), pp. 243–263. ISSN: 1873-9326. DOI: 10.1007/s11869-015-0338-3. URL: https://doi.org/10.1007/s11869-015-0338-3.

[26] "Appendixes: Computer Programs". In: *Absorption and Scattering of Light by Small Particles*. John Wiley Sons, Ltd, 2007, pp. 475–476. ISBN: 9783527618156. DOI: 10.1002/9783527618156.app1. eprint: https://onlinelibrary.wiley.com/doi/pdf/10.1002/9783527618156.app1. URL: https://onlinelibrary.wiley.com/doi/abs/10.1002/9783527618156.app1.

[27] Michael Hess, Peter Koepke, and I Schult. "Optical properties of aerosols and clouds: The software package OPAC". In: *Bulletin of the American meteorological society* 79.5 (1998), pp. 831–844.

[28] GR Meira et al. "Modelling sea-salt transport and deposition in marine atmosphere zone–A tool for corrosion studies". In: *Corrosion Science* 50.9 (2008), pp. 2724–2731.

[29] Rodrigo Munoz-Alpizar et al. "Multi-year (2013–2016) PM2. 5 wildfire pollution exposure over North America as determined from operational air quality forecasts". In: *Atmosphere* 8.9 (2017), p. 179.

[30] JM Walker et al. "Simulation of nitrate, sulfate, and ammonium aerosols over the United States". In: *Atmospheric Chemistry and Physics* 12.22 (2012), pp. 11213–11227.

[31] Yi Li et al. "Increasing importance of deposition of reduced nitrogen in the United States". In: *Proceedings of the National Academy of Sciences* 113.21 (2016), pp. 5874–5879.

[32] Amara L. Holder et al. "Particulate matter and black carbon optical properties and emission factors from prescribed fires in the southeastern United States". In: *Journal of Geophysical Research: Atmospheres* 121.7 (Apr. 2016), pp. 3465–3483. ISSN: 2169897X. DOI: 10.1002/2015JD024321. URL: http://doi.wiley.com/10.1002/2015JD024321.

[33] Douglas H Lowenthal and Naresh Kumar. "Variation of Mass Scattering Efficiencies in IMPROVE". In: *Journal of the Air & Waste Management Association* 54.8 (2004), pp. 926–934. ISSN: 2162-2906. DOI: 10.1080/10473289.2004.10470969. URL: https://www.tandfonline.com/action/journalInformation?journalCode=uawm20.

[34] Easan Drury et al. "Synthesis of satellite (MODIS), aircraft (ICARTT), and surface (IMPROVE, EPA-AQS, AERONET) aerosol observations over eastern North America to improve MODIS aerosol retrievals and constrain surface aerosol concentrations and sources". In: *Journal of Geophysical Research* 115.D14 (July 2010), p. D14204. ISSN: 0148-0227. DOI: 10.1029/2009JD012629. URL: http://doi.wiley.com/10.1029/2009JD012629.